Article

Not peer-reviewed version

# Power Flow in Coupled Three-Row Series-Parallel Planetary Gear System. Part I: Without Power Losses

Józef Drewniak *, Tomasz Kądziołka *, Jacek Rysiński, Konrad Stańco

Posted Date: 3 August 2023

doi: 10.20944/preprints202308.0223.v1

Keywords: compound and coupled planetary gear systems; series-parallel planetary gear systems; power flow; circulating power flow

*Article*

# Power Flow in Coupled Three-Row Series-Parallel Planetary Gear System. Part I: Without Power Losses

**Józef Drewniak [1,*], Tomasz Kądziołka [2,*], Jacek Rysiński [1] and Konrad Stańco [1]**

[1] Faculty of Mechanical Engineering and Computer Science, University of Bielsko-Biała; 43-309 Bielsko-Biała, Poland
[2] Faculty of Engineering Sciences, University of Applied Sciences, 33-300 Nowy Sącz, Poland
* Correspondence: jdrewniak@ath.bielsko.pl; tkadziolka@ans-ns.edu.pl

**Abstract:** Comparisons of power flows and efficiencies in two structurally quite similar cylindrical series-parallel planetary gear systems (PGSs) were performed in three separate parts of this paper. Each of these single degree of freedom (DoF) systems consists of three different 2KH subsystems connected in series-parallel. The main goal was to prove that apart from complex, structurally and dynamically coupled PGSs, there are also complex and only structurally coupled PGSs, in which the phenomenon of power flow circulation inside closed loops does not occur. Such a half-coupled type of PGS is herein called pseudo-coupled. Therefore, Part I discusses in detail the geometry, kinematics and statics of coupled PGSs in order to determine power flow paths. A comparison of the directions of power flow in both types of PGSs can be made in Part II after determining the power flow paths in the second planetary gear in a similar way. The directions of power flow in both types of PGSs were determined in a relatively simple way, thanks to the distinction between active and passive torques and thus active and passive shafts of individual subsystems. The efficiency comparison made in Part III will show whether power circulation has an influence on the efficiency value, at least in these two types of PGSs.

**Keywords:** compound and coupled planetary gear systems; series-parallel planetary gear systems; power flow; circulating power flow

## 1. Introduction

Cylindrical series-parallel planetary gear systems (PGSs) are a special variety of complex and most commonly coupled planetary transmissions. They consist of at least two subsystems (units) in the form of elementary 2KH planetary gears connected in parallel and possibly in series. Each of the subsystems connected in parallel has mobility equal to two [1-6]. This means that they have all the gears moving along with the carriers. On the other hand, subsystems connected in series have mobility equal to 1, which means that they can work as typical planetary type with stationary rim gear. Very rarely, these are solar-type units with stationary sun gear or star-type units, i.e. multi-path with fixed satellite axes due to the stationary carrier. Depending on the number and types of subsystems connected in series, the entire series-parallel gearbox may have a mobility of 1 to 3. They are characterized by the fact that they have multiple paths of power transmission, which may cause the phenomenon of power closure inside at least one parallel connected elementary subsystem. Such power coupling in the form of its circulation [7-11] can be a source of even a large overload of gears, shafts and/or bearings of a closed subsystem. In the case of an unfavorable distribution of power on individual paths, an additional reduction in efficiency may be revealed. Therefore, after determining the directions of power flow, power losses caused by friction in the meshing and efficiency should be determined.

This important problem was mentioned as early as in 1928 by Buckingham in the book [12], while H. Brandenberger is the author of the publication [13] from 1929, in which, on the occasion of calculating the efficiency of complex planetary gears, he proposed an analytical method of determining the directions of power flow. Then the power flow problem was subsequently made available in improved versions of analytical methods in books [13-24]. The analytical method uses

three basic equations of planetary transmissions, i.e. kinematics equation (usually the Willis dependence), statics equation (moment balance equation) and energy (power) balance equation. Thus, this method allows for direct analysis of kinematics, statics and thus for direct identification of power flow directions in coupled planetary gears with mobility of one or more [25-40], in automatic gearboxes [41-50] and in power-split hybrid systems consisting of planetary units with mechanical or hydro-mechanical continuously variable transmissions (CVT) [51-76] or in power-split hybrid electric vehicle (PSHEV) planetary transmission in single-motor (1-PG) or two-motor (2-PG) versions, sometimes with an additional internal combustion engine (ICE) [77-128]. In the last two types of transmission, i.e. in the power-split powertrain (with CVT applied, but without an additional motor) and PSHEV planetary transmission, the power flow occurs as power splitting and power circulation. A great facilitation of the analysis of such gear trains, as well as complex and coupled gear transmissions with any possible mobility, is the possibility of their decomposition into elementary subsystems, called blocks, branches or geared entities [53, 54, 56, 57, 72, 106, 214]. In the first modified version of the analytical method, the kinematics and statics are analyzed using the matrix method, which makes the form of equations more compact and easier to perform computer calculations [129, 130]. In an equally popular variant, angular velocities and torques are determined using the lever analogy method and nomograms [131-139]. The analytical geometry method [140] consists in plotting circuit relationship graph (circuit lines on the angular speed plane) and circuit relationship graph with kinetic energy increment. The dimensionless angular velocity and dimensionless virtual angular velocity obtained respectively from these circuit relationship graphs, allow to determine the angular velocities, velocity ratios, torques, power flow and meshing efficiency of any planetary gear [141]. Also very interesting is the combined method of determining power flow and efficiency epicyclic transmission presented in Refs. [142-151], where the Lagrange multipliers and kinematic constraints are used to determine the power flow and to verify the normal power flow balance. Accuracy is increased by including virtual power in the analysis, where *virtual power* was determined in a non-inertial frame of epicyclic planetary gear.

The method based on the graph representation of planetary gears (based on the graph representation) is the best technique for analysing kinematics, statics and thus detecting the directions of power flow. The kinematic analysis of planetary gear trains is largely simplified. This applies in particular to complex and coupled planetary gear transmissions with mobility equal any number, automatic transmissions, power-split hybrid systems and power-split hybrid electric vehicles. Interactive computer programs for the global analysis of kinematics, statics and identification of active and passive gears, i.e. power flow directions, are very helpful and easy to develop. The most commonly used are undirected graph, directed graph, topological graphs, hypergraphs, signal flow graphs and bond graphs [90, 152-172]. Graphs or hypergraphs methods can be combined with the matrix method [84, 199]. There are also papers in which graphs were used primarily to synthesize the structure of the gear with the required ratio and possibly to determine the angular velocity, while the torques of the wheels and arms were determined by the method of torque balance or matrix, lever analogy or other techniques.

The above review of the literature shows that when determining the directions of power flow in complex series-parallel transmissions, no cases of the lack of power circulation in closed loops were identified. Therefore, this paper will present the method of using the analytical, i.e. the classical method for determining the directions of power flow of power losses in such complex planetary gears. By the way, a serious difference in the values of loads on gears and carriers of two series-parallel gears, very similar in terms of structure, will be shown.

The rest of this paper is as follows. Section 2 (Materials and Methods) discusses in detail the problem of dividing complex serial-parallel PGSs into subsystems and familiarizes with the analytical method of determining the active and passive shafts of each subsystem, i.e. paths and directions of power flow. This method was used in Section 3 (Case study), where angular velocities, active and reaction torques as well as active and passive subsystem shafts were determined for the coupled and complex serial-parallel PGS. Verifying calculations of angular velocities, torques and powers along with power ratios are presented in Appendices A, B, C and D. The final result of the

 doi:10.20944/preprints202308.0223.v1



analysis is shown in Figure 9. However, the main comments regarding the analysis are given in Conclusions.

## 2. Materials and Methods

### *2.1. Kinematic and block models of series-parallel PGSs*

#### 2.1.1. Geometric structure of series-parallel PGSs

Complex planetary gear systems can be divided into series and series-parallel gear systems (PGS) [18, 23]. Series gears are multi-stage gear systems, consisting of at least two single-stage gear subsystems called stages. Each gear stage, like the entire gear system, has mobility equal to one, which means that there is only one way to transmit the power stream. Therefore, in a relatively simple way, it is possible to carry out not only an analysis of the kinematics and statics of such gears, but also an assessment of power losses and efficiency. For example, the total gear ratio and the gear efficiency of a series gear resulting only from the power losses in the meshing are, respectively, the products of the gear ratios and the efficiency of the individual stages.

Cylindrical PGSs are complex closed mechanisms and therefore are called coupled planetary gears with a mobility of at least one. They consist of at least one elementary planetary gear connected in parallel, hereinafter referred to as a subsystem, not a stage . Such complex and coupled gears are characterized by a constant ratio of relatively high value (Figure 1(a)). Methods of their synthesis are presented in [18-20, 22, 23]. Due to the series-parallel structure of such gears, they cannot be divided into kinematic stages, which means that their analysis cannot use the facilities associated with multi-stage gears. Therefore, due to this and a more complex structure, they have not found such wide application in industrial practice as series multi-stage planetary gears. On the other hand, modified types of series-parallel gear systems are very popular. It is possible to attach an additional subsystem to such transmissions in the form of mechanical or hydro-mechanical CVT, thanks to which the obtained ratio can change continuously. In the synthesis process, series-parallel transmissions can also be relatively easily converted into step-variable transmissions, i.e. automatic gearboxes or power split hybrid electric vehicle planetary transmission in single-, two- and even three-motor versions plus one internal combustion engine (ICS). An example may be a gearbox with several gears (Figure 1(b)) obtained from the transformation of the series-parallel gearbox shown in Figure 1(a). Other examples of such gearboxes are presented, for example, in papers [44, 77, 97, 98, 127, 135, 138, 161, 202, 207, 208,209].

Most series-parallel transmissions are structurally and dynamically coupled. However, there are also only structurally coupled gear systems due to the fact that their subsystems connected in parallel have the form of closed loops. Dynamically coupled gears are characterized by the fact that part of their power locked in these loops simultaneously circulates in them [7-11, 31, 35, 64, 102]. In Part I of this paper, only series-parallel transmission is analysed, which turns out to be structurally and dynamically coupled.

Figure 1 shows an exemplary kinematic diagram of a complex and coupled PGS. This system consists of three main shafts I, II and III. In the case of a reduction gear with mobility equal to one, the shaft I is the input shaft, the shaft II is the output shaft, and the hollow shaft III is fixed. When all three shafts are moving together with the ring gear 9, the gear has a mobility of two. The gear system consists of three sun gears 1, 4 and 7, three sets of planet gears 2, 5 and 8, three rim gears 3, 6, 9 and three carriers $h_2$, $h_5$ and $h_8$.

Preprints (www.preprints.org) | NOT PEER-REVIEWED | Posted: 3 August 2023 doi:10.20944/preprints202308.0223.v1



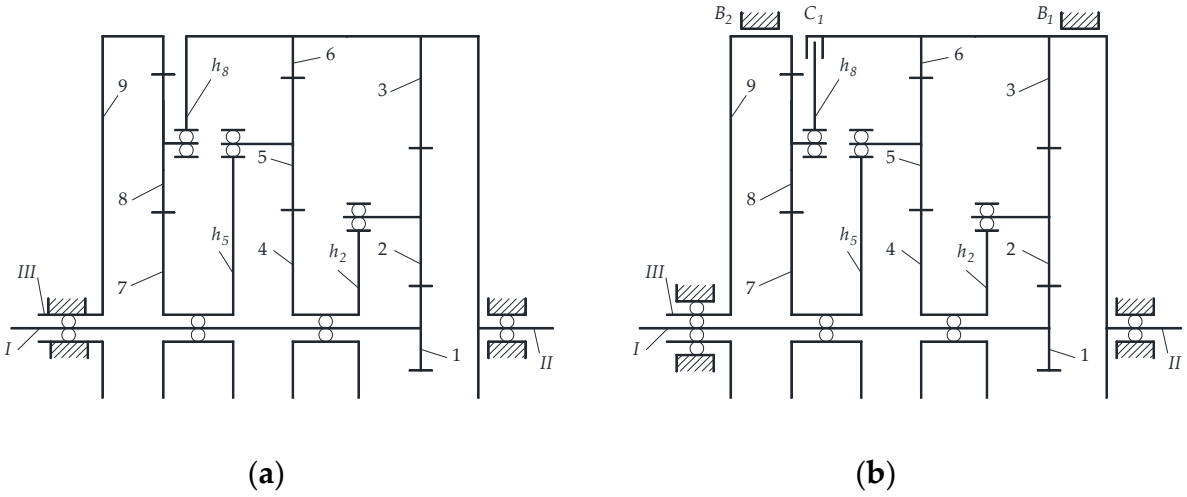


**Figure 1.** Kinematic diagrams of (**a**) PGS and (**b**) automatic gear train.

Mobility is an important parameter of each planetary gear, including each of its subsystems. This is the number of constraints that should be imposed on the kinematic chain composed of gear elements in order to lock it. The measure of mobility is therefore the number of DoF relative to the stationary base. In practice, however, it is the number of drives (input shafts) that must ensure a strictly defined movement of all its moving elements (gears and carriers). Thus, the number of independent input motions must equal the number of DoF, so that the basic condition of its correct structure, i.e. no redundant members, is ensured. The analysed cylindrical planetary gears are planar mechanisms, so their mobility $M$ calculated from the formula [1, 198]:

$$M = 3 \cdot n - 2 \cdot p_5 - p_4 , \qquad (1)$$

where $n$ is the number of active members, i.e. without frames, $p_5$ - number of lower pairs, i.e. with one DoF, $p_4$ - number of higher pairs, also called half pairs, i.e. with two DoF.

A characteristic feature of the series-parallel transmission shown in Figure 1 is that it comprises two closed loops. The first loop is bounded by carrier $h_2$ and the gears 2, 3, 6, 5 and 4, while the second loop is bounded by carrier $h_5$ and the gears 5, 6, 7 and 8. In the closed loops of most PGSs, power can circulate in a direction that can be determined by the method presented in this paper. In the exemplary transmission (Figure 1), all directions of power flows are possible with two exceptions. Namely, in the first loop, the power flows on carrier $h_2$ and rim gear 3, cannot be directed towards each other at the same time (they cannot converge), as well as the power flows on rim gear 6, and carrier $h_8$ in the second loop. The power circulating in a closed loop can even exceed the power applied to the subsystem, which can cause a devastating overload of the gears.

2.1.2. Decomposition of series-parallel gear system into subsystems

The series-parallel gear system can be decomposed into subsystems in the form of separate single planetary gears with mobility equal to 2 or 1, i.e. subsystems with two or one DoF respectively. The condition for including the planetary gear in the family of series-parallel gears is the possibility of separating from it at least one subsystem with the number of two DoF.

Figure 2(a), (b), (c), (d), (e), (f) shows six basic types of two DoF subsystems in block form [52-54, 56, 57, 214]. Each of these subsystems consists of a sun gear, rim gear and carrier (hidden in the block as in a "black box") and three movable shafts. At least one of these shafts must be the input shaft to the subsystem, i.e. the active shaft marked with an arrow pointing towards the block, and at least one - the output shaft of the subsystem, i.e. the passive shaft marked with an arrow pointing outwards

Preprints (www.preprints.org) | NOT PEER-REVIEWED | Posted: 3 August 2023 doi:10.20944/preprints202308.0223.v1



from the block. In addition, individual shafts are marked with the letters α, β, h, and specifically the letter α - sun gear shaft, the letter β - rim gear shaft and the letter h - carrier shaft.

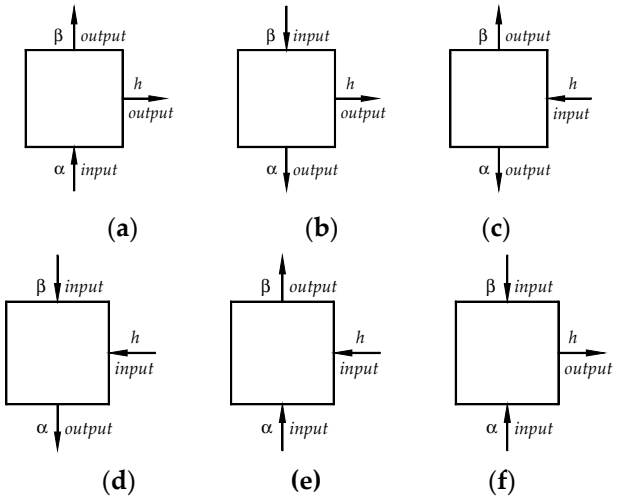


**Figure 2.** Block diagrams of possible types of subsystems with two DoF.

In Figure 3, six basic types of subsystems with a single DoF are presented in block form. Also here, each of the subsystems, just like each stage in a multi-stage planetary gear (series), consists of a sun gear, a rim and several planet gears and a carrier (hidden in the block as in a "black box") and three coaxial shafts, one of which is it is locked together with the internal element of the subsystem connected to it. Thus, in a single DoF subsystems, only one shaft is active and one shaft is passive. The designations of these shafts are the same as the shafts in the two DoF subsystems. Subsystems with a fixed carrier (Figure 3(b), (d)) are multipath gears with fixed planet gear axes (so-called star gears).

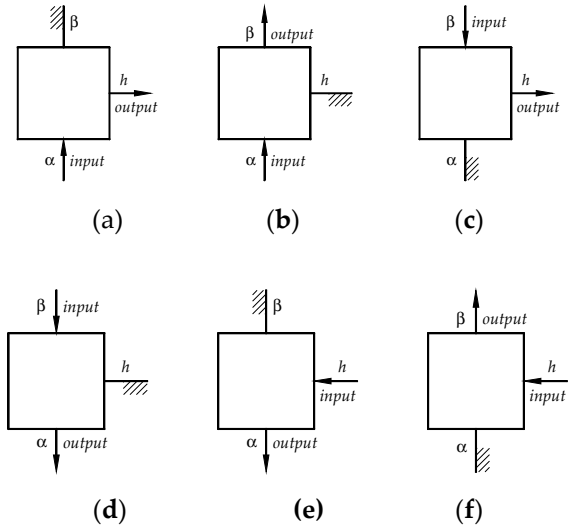


**Figure 3.** Block diagrams of possible types of single DOF subsystems.

*2.2. Analysis algorithm of the power stream flow in PGS without power loss*

2.2.1. Method algorithm

During operation, the shafts of the subsystems of series-parallel planetary gear may rotate in directions consistent with or opposite to the directions of torque action. In the case of matching turns, the power on the shaft is called active power transferred to the analysed subsystem, and when the turns are opposite - reactive power transferred outside the subsystem. Since the power on the shaft

is equal to the product of angular velocity and torque, active power is assigned a plus sign ("+"), and reactive power - a minus sign ("-").

The above simple principle is the basis for determining the flow directions of power streams in closed and complex planetary gears. It is enough to distinguish the active power from the reactive power and, accordingly, the active shaft from the passive one. Of course, each subsystem must have at least one active shaft and one passive shaft. In practice, determining the active and passive shafts in each subsystem is quite a laborious task, because beforehand, a detailed analysis of kinematics, i.e. determination of angular velocities) and statics, i.e. determination of torques without taking into account power losses, should be carried out.

A detailed algorithm for determining the direction of power flow is presented below:

a) gearbox geometry analysis - determination of gearbox mobility (1), decomposition of the gearbox into kinematic subsystems and their classification depending on the number of DoF - Figure 2, Figure 3, subsections 3.1 and 3.2,
b) determination of the magnitudes and directions of angular velocities of gears and carriers in subsequent subsystems - subsubsections 2.2.3, 3.3.1 and Appendices A, B,
c) determination of the magnitudes and directions of action of the torques loading the shafts of each of the subsystems (at this stage of calculations, without taking into account power losses) – subsubsections 2.2.4, 3.3.3 and Appendix C,
d) determining the active and passive shafts of each of the transmission subsystems and the directions of the flow of power streams – subsubsections 2.2.5, 3.3.4, 3.3.5.

Knowing the directions of power flow in each of the subsystems, it is possible to determine the torques and powers, taking into account friction in the meshing as well as power losses and transmission efficiency. The solution to this problem will be presented in Part III of this paper.

### 2.2.2. Analysis of the geometry of series-parallel gear systems and classification of its components

The presented method of identifying the directions of power flow of the analysed PGS, and later (in Part III) also power losses, consists in determining these directions and power losses separately for each subsystem from the input to the output of the gear. It is therefore necessary to start the analysis by dividing the gear into subsystems and determining their mobility. The classification of subsystems is carried out on the basis of the number of DoF in accordance with the formula (1). The method of dividing the example series-parallel transmission (Figure 1) into subsystems and the classification of possible subsystems of such transmissions (Figure 2 and Figure 3) are discussed in subsubsection 2.1.1. A detailed analysis of the geometry of the gear subsystems (Figure 4) was carried out in subsection 3.1.

### 2.2.3. Analysis of the kinematics of series-parallel gears

In order to determine the directions of the flow of power streams and to estimate the power losses in the meshing, it is necessary to determine the magnitudes and directions of the angular velocity vectors of the gears and carriers of each gear subsystem in advance (blocs, units or branches) [214]. In practice, the Willis formula [14-23, 191, 207, 217] is often used for this purpose, although graph methods (linear, contour, signal flow, bond graphs, matroids and hypergraphs) are gaining more and more recognition, thanks to their advantages [153, 174, 175, 177-182, 184-190, 192-200, 203, 206, 207, 210, 212-216, 218]. The nomograph method and especially lever analogy are also promising as universal methods for kinematics, statics and power flow analysing of the most complex PSHEV planetary transmission [176, 201-203, 211]. The effectiveness of the above-mentioned methods can be additionally increased by the matrix notation of the obtained equations [204, 211, 215].

Angular velocities of gears and carriers of analysed PGS subsystems are determined in subsubsections 3.3.1. A detailed analysis of the kinematics of these gears is presented in Appendices A, B. For this purpose, Willis formulas and other kinematic relations were used, which are briefly presented below. By the way, the method of saving individual parameters was also explained.

Preprints (www.preprints.org) | NOT PEER-REVIEWED | Posted: 3 August 2023 doi:10.20944/preprints202308.0223.v1



The gear ratio $i_{a,p}$ of each gear transmission, both with fixed axes and planetary gear with the single DoF, i.e. gears containing one active a and one passive p shaft, is determined from the formula:

$$i_{a,p} = \frac{\omega_a}{\omega_p}, \tag{2}$$

where $\omega_a$ and $\omega_p$ are the absolute angular velocities of the active and passive shafts, respectively, i.e. in motion relative to the stationary gear housing.

Two Willis formulas for two drive directions in the analyzed subsystems are presented below:

$$i^h_{\alpha,\beta} = \frac{\omega^h_\alpha}{\omega^h_\beta} = \frac{\omega_\alpha - \omega_h}{\omega_\beta - \omega_h} \quad \text{or} \quad i^h_{\beta,\alpha} = \frac{\omega^h_\beta}{\omega^h_\alpha} = \frac{\omega_\beta - \omega_h}{\omega_\alpha - \omega_h}, \tag{3}$$

where $i^h_{\alpha,\beta}$ is the *stationary transmission ratio* (otherwise *fixed carrier gear ratio),* i.e. determined in the reference system associated with the carrier h, binding the angular velocity $\omega^h_\alpha$ of the active shaft with the sun gear $\alpha$ and the angular velocity $\omega^h_\beta$ of the passive shaft with rim gear $\beta$, while $i^h_{\beta,\alpha}$ is the *fixed carrier gear ratio*, binding the angular velocity $\omega^h_\beta$ of the active shaft with rim gear $\beta$ and the angular velocity $\omega^h_\alpha$ of the passive shaft with sun gear $\alpha$.

In this way, two Willis formulas were derived for two possible directions of transmission of the drive, respectively from the shaft with the sun gear $\alpha$ to the shaft with the rim gear $\beta$ and vice versa in the reference system related to the carrier shaft h. The *fixed carrier gear ratios* $i^h_{\alpha,\beta}$ and $i^h_{\beta,\alpha}$ can also be expressed by geometric formulas depending on the type and number of teeth of the sun and rim gears of the subsystem, such as for type 2K-H:

$$i^h_{\alpha,\beta} = \left(-\frac{z_\gamma}{z_\alpha}\right)\cdot\left(-\frac{z_\beta}{z_\gamma}\right) = \frac{z_\beta}{z_\alpha} \quad \text{or} \quad i^h_{\beta,\alpha} = \left(-\frac{z_\gamma}{z_\beta}\right)\cdot\left(-\frac{z_\alpha}{z_\gamma}\right) = \frac{z_\alpha}{z_\beta}. \tag{4}$$

where $z_\alpha$, $z_\gamma$, $z_\beta$ are the tooth numbers of the sun, planet and rim gears, respectively. Comparing the left-hand sides of formulas (3) and (4) gives practical forms of Willis equations:

$$\frac{\omega_\alpha - \omega_h}{\omega_\beta - \omega_h} = \frac{z_\beta}{z_\alpha} \quad \text{or} \quad \frac{\omega_\beta - \omega_h}{\omega_\alpha - \omega_h} = \frac{z_\alpha}{z_\beta}. \tag{5}$$

The magnitudes and directions of the unknown angular velocity vectors of the gears and carriers are determined from a system of equations of the type (5) derived for each of the subsystems of the PGS and supplemented with equations enabling the determination of the position of instant centers of rotation (Appendix B).

2.2.4. Static analysis without taking into account meshing friction

To determine the active and passive shafts of each of the subsystems of the PGS, and thus to determine the directions of power flow, it is necessary to determine the magnitudes and directions of the torque vectors acting on the shafts of sun gears, ring gears and carriers of each subsystem. At this stage of calculations, it is possible to determine the magnitudes and directions of torque without taking into account power losses using graphical and analytical methods, including free body diagram [184, 185] and lever or nomograph methods [176, 201-203, 211]. The most popular techniques due to the possibility of automating calculations are the methods of classical directed or undirected graphs, signal graph and contour graphs [18, 154, 159, 175, 192]. In Appendix C of this paper, the free body diagram method was used. Especially in order to facilitate the detection of the active and passive shafts of the subsystems, reaction torques have been additionally included. However, on the

Preprints (www.preprints.org) | NOT PEER-REVIEWED | Posted: 3 August 2023 doi:10.20944/preprints202308.0223.v1



basis of only the data determined so far (angular velocities and torques), it is difficult to distinguish the active shaft(s) from the passive shaft(s). It is best to additionally use the equation of moment equilibrium and energy balance.

2.2.5. Identification of active and passive shafts and power flow directions

It is known that the dot product of the same-directed vectors of torque and angular velocity $\mathbf{T}_j \cdot \boldsymbol{\omega}_j > 0$, where $j = \alpha, \beta, h$, i.e. power $P_j > 0$ is active, and this means that power is supplied to the subsystem through the active shaft. In the case of these vectors oppositely directed, their product $\mathbf{T}_j \cdot \boldsymbol{\omega}_j < 0$, i.e. the power $P_j < 0$ is reactive and this means that the power is discharged from the subsystem through the passive shaft. Then, the torque vector is a reaction torque, marked $\mathbf{T}_{jR}$ as the resistance moment of the shaft of the adjacent driven subsystem. Thus, when identifying the active and passive shafts of subsystems connected in series or in parallel, two basic conditions for transferring power from or to a subsystem are used:

(1) for the driving shaft, the vectors of the angular velocity $\boldsymbol{\omega}_j$ and the torque $\mathbf{T}_j$ are in the same direction ($\mathbf{T}_j \cdot \boldsymbol{\omega}_j > 0$),

(2) for the driven shaft, the vectors of the angular velocity $\boldsymbol{\omega}_j$ and the reaction torque $\mathbf{T}_{jR}$ are oppositely directed ($\mathbf{T}_j \cdot \boldsymbol{\omega}_j < 0$).

Unfortunately, these are only the conditions necessary to be met. Sufficient conditions is a system of governing equations derived separately for each of the subsystems with mobility equal to 1 or 2. Each such system consists of a torque equilibrium equation and practically one energy balance equation in the reference system related to the stationary body, because the second equation of the energy balance in the system associated with the carrier can only be used for verification. A certain difficulty in deriving these equations for the subsystem with mobility equal to 2 is the lack of identified characters of the two shafts (Figure 2). The nature of the third shaft is known because it is either the input or output shaft of the PGS, or it is an extension of the shaft of the adjacent subsystem whose shafts have been identified earlier (Figure 4 to Figure 7). If for instance the shaft of an adjacent subsystem is passive, then the shaft of the analyzed subsystem is active.

In the general case, there are three versions of the governing equations, assuming that the shaft of the sun gear is active.

First version modelling the type 2(a) subsystem:

$$T_\alpha + T_{\beta R} + T_{hR} = 0, \tag{6}$$

$$T_\alpha \cdot \omega_\alpha + T_{\beta R} \cdot \omega_\beta + T_{hR} \cdot \omega_h = 0, \tag{7}$$

where conditions for active and passive shafts are as follows: $T_\alpha \cdot \omega_\alpha > 0$, $T_{\beta R} \cdot \omega_\beta < 0$ and $T_{hR} \cdot \omega_h < 0$.

Second version modelling the type 2(e) subsystem:

$$T_\alpha + T_{\beta R} + T_h = 0, \tag{8}$$

$$T_\alpha \cdot \omega_\alpha + T_{\beta R} \cdot \omega_\beta + T_h \cdot \omega_h = 0, \tag{9}$$

where conditions for active and passive shafts are as follows: $T_\alpha \cdot \omega_\alpha > 0$, $T_{\beta R} \cdot \omega_\beta < 0$ and $T_{hR} \cdot \omega_h > 0$.

Third version modelling the type 2(f) subsystem:

$$T_\alpha + T_\beta + T_{hR} = 0, \tag{10}$$

$$T_\alpha \cdot \omega_\alpha + T_\beta \cdot \omega_\beta + T_{hR} \cdot \omega_h = 0, \tag{11}$$

Preprints (www.preprints.org) | NOT PEER-REVIEWED | Posted: 3 August 2023 doi:10.20944/preprints202308.0223.v1



where conditions for active and passive shafts are as follows: $T_\alpha \cdot \omega_\alpha > 0$ , $T_\beta \cdot \omega_\beta > 0$ and $T_{hR} \cdot \omega_h < 0$ .

The fourth version with three active shafts is impossible to implement, both from a mathematical and technical point of view. Reasons: the positive terms of the sum cannot be zero and each gear transmission must have at least one input and one output.

Using the "trial and error" method, it is possible to choose the right version of governing equations, because the magnitude of active $T_j$ and reactive torques $T_{jR}$, as well as the products of torques and angular velocities ( $T_j \cdot \omega_j > 0$ ) and ( $T_{jR} \cdot \omega_j < 0$ ) are known.

Of course, in the case of subsystems with mobility equal to 1, there is no problem with identifying the power flow path, because such a subsystem depending on the type (Figure 3) has known input and output shafts. Moreover, its third shaft is fixed and hence its angular velocity and power are respectively $\omega_j = 0$ and $P_j = T_{jR} \cdot \omega_j = 0$ , where $j = \alpha$ , $\beta$ or h. Then the subsystem equilibrium equations are determined directly without fitting the conditions for active and passive shafts with one of the three versions of the equations ((6),(7)), ((8), (9)) or ((10), (11)).

The directions of power flow in PGS are independent of whether power losses are taken into account or not when calculating the torques. The reason is that the active and reactive torque vectors calculated without taking into account the power losses $\mathbf{T}_j$ and $\mathbf{T}_{jR}$, respectively, differ only in magnitude from the corresponding torque vectors calculated taking into account these losses $\tilde{\mathbf{T}}_j$ and $\tilde{\mathbf{T}}_{jR}$, respectively. This will be demonstrated in Part III of this paper.

The active and passive shafts of the transmission subsystems of the PGS determined in the above manner are presented in subsubsection 3.3.4, based on the data collected in Table 6 to Table 9 and Figure 6 to Figure 8.

## 3. Case Study

### *3.1. Case study subjects*

The purpose of this chapter is to present in detail the graphical and analytical method of determining the directions of power stream flow in PGS. In Part II will be presented a very similar planetary gear in terms of geometric structure. However, such important parameters as gear ratios $i_{in,out}$, input angular velocities $\omega_1$ and input torques $T_1$ of both systems will be the same. The forms of PGSs have been specially selected so that their kinematic and dynamic similarities and differences could be demonstrated.

Figures 4 shows the diagrams of analysed PGSs in forms of (**a**) kinematic and (**b**) block.

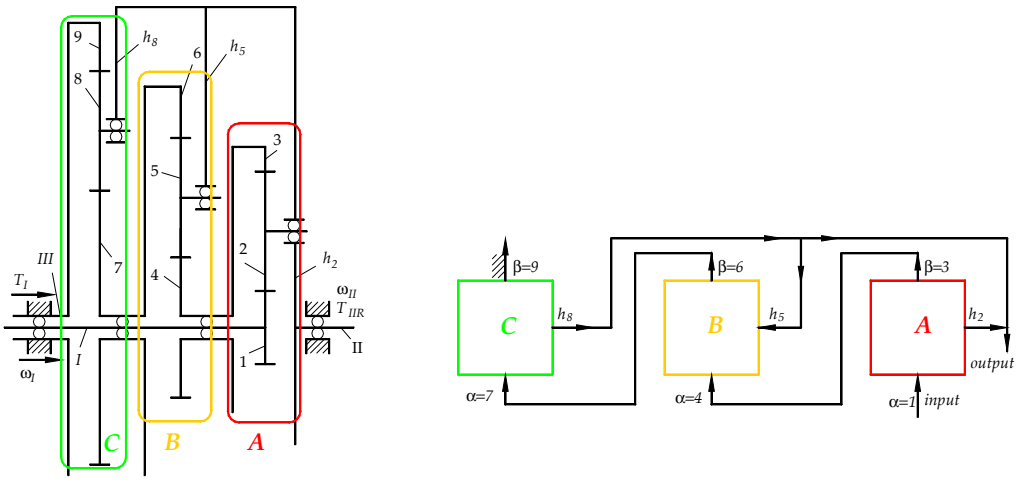


**(a)** **(b)**

Preprints (www.preprints.org) | NOT PEER-REVIEWED | Posted: 3 August 2023 doi:10.20944/preprints202308.0223.v1



**Figure 4.** Diagrams of the analysed PGS (**a**) – Kinematic, (**b**) – Block.

The subsystem blocks A, B, C are additionally separated in the kinematic diagrams in Figure 6 and Figure 7. The names of subsystem types (according to Figure 2 and Figure 3) are shown in Table 1. For example, the subsystem A of type (2a) belonging to analysed PGS corresponds to the block shown in Figure 2(a).

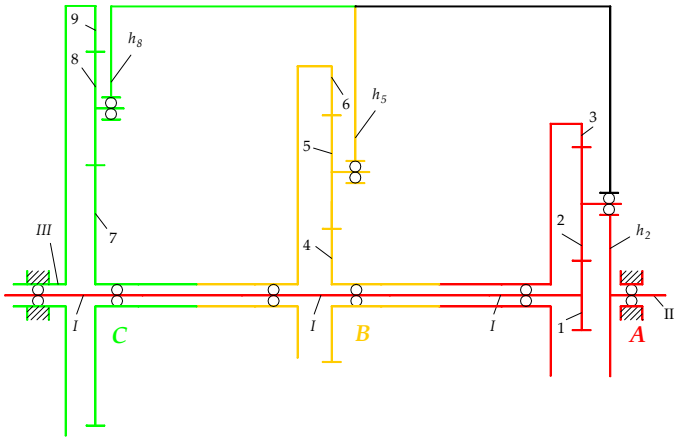


(**a**) (**b**) (**c**)

**Figure 5.** Kinematic diagrams of analysed PGS subsystems C, B, A.

**Table 1.** Numbers of DoF of the PGS subsystems.

| **Subsystem** | A | B | C |
|---|---|---|---|
| DoF | 2 | 2 | 1 |
| Subsystem type | 2(a) | 2(e) | 1(a) |

All blocks shown in Figure 2 correspond to three-shaft subsystems, i.e. they contain three moving shafts and thus have two DoF each. On the other hand, all blocks shown in Figure 3 correspond to two-shaft subsystems, i.e. they contain two movable shafts and thus have one DoF each.

*3.2. Data*

Table 2 presents data on the geometry of the gears of the analysed PGS.

Parameter symbols:

$z_i$, $d_i$, $m_i$ - number of teeth and pitch diameters and gear modules ($i = 1$ to 9),

$r_{h_j}$, $s_j$ - carriers radii and number of planet gears ($j = 2, 5, 8$), respectively. There is also input torque $T_1 = 10\,\mathrm{N\cdot m}$ and input angular velocity (rotation velocity) $\omega_1 = 153.938\,\mathrm{rad/s}$ ($n_1 = 1470\,\mathrm{RPM}$).

**Table 2.** Data on PGS.

| Subsystem A | | | Subsystem B | | | Subsystem C | | |
|---|---|---|---|---|---|---|---|---|
| $z_1 = 18$ | $z_2 = 72$ | $z_3 = -162$ | $z_4 = 18$ | $z_5 = 99$ | $z_6 = -216$ | $z_7 = 24$ | $z_8 = 99$ | $z_9 = -222$ |
| $d_1 = 18$ | $d_2 = 72$ | $d_3 = -162$ | $d_4 = 27$ | $d_5 = 148.5$ | $d_6 = -324$ | $d_7 = 60$ | $d_8 = 247.5$ | $d_9 = -555$ |
| $m_A = m_1 = m_2 = m_3 = 1\mathrm{mm}$ | | | $m_B = m_4 = m_5 = m_6 = 1.5\mathrm{mm}$ | | | $m_C = m_7 = m_8 = m_9 = 2.5\ \mathrm{mm}$ | | |
| $r_{h_2} = (d_1 + d_2)/2 = 45\mathrm{mm}$ | | | $r_{h_5} = (d_4 + d_5)/2 = 87.75\mathrm{mm}$ | | | $r_{h_8} = (d_7 + d_8)/2 = 153.75\mathrm{mm}$ | | |
| $s_2 = 3$ | | | $s_5 = 3$ | | | $s_8 = 3$ | | |

Preprints (www.preprints.org) | NOT PEER-REVIEWED | Posted: 3 August 2023 doi:10.20944/preprints202308.0223.v1



| | |
|---|---|
| $T_I = T_1 = 10\ \mathrm{N \cdot m}$ | $\omega_I = \omega_1 = 153.938\ \mathrm{rad/s}\ \ (n_I = n_1 = 1470\ \mathrm{RPM})$ |

*3.3. Power flow paths in PGS*

3.3.1. Calculations of angular and tangential velocities

The values of the fixed *carrier transmission ratios* of the subsystems A, B, C and pairs of sun and planet gears are listed in Table 3 based on calculations in Appendix A. These parameters are necessary to determine the angular velocity of the gears and the carriers of the PGS.

**Table 3.** Values of *fixed carrier transmission ratio* of subsystems of analysed PGS.

| $i_{1,3}^{h_2} = z_3/z_1$ | $i_{4,6}^{h_5} = z_6/z_4$ | $i_{7,9}^{h_8} = z_9/z_7$ | $i_{1,2}^{h_2} = -z_2/z_1$ | $i_{4,5}^{h_5} = -z_5/z_4$ | $i_{7,8}^{h_8} = -z_8/z_7$ |
|---|---|---|---|---|---|
| –9 | –12 | –9.25 | –4 | –5.5 | –4.125 |

*Designations of fixed carrier transmission ratios* from Table 5: $i_{1,3}^{h_2}$, $i_{4,6}^{h_5}$, $i_{7,9}^{h_8}$ - the ratios of the subsystems A, B, C, respectively, $i_{1,2}^{h_2}$, $i_{4,5}^{h_5}$, $i_{7,8}^{h_8}$ - the ratios of the sun – planet gear pairs $1-2$, $4-5$ and $7-8$, respectively.

Detailed calculations of the angular and tangential velocities of sun, ring, planet gears and carriers are provided in Appendices A and B. In addition, the angular velocity magnitudes are presented in Table 4 and their directions are shown in Figure 8 to Figure 10 and Figure B1 to Figure B3. Also the direction of tangential velocity vectors are shown in Figure B1 to Figure B3 and their magnitudes in Table B1 and Table B2.

**Table 4.** Magnitudes of angular velocities of the PGS in $\mathrm{rad/s}$.

| $\omega_{II} = \omega_{h_2} = \omega_{h_5} = \omega_{h_8}$ | $\omega_2$ | $\omega_3 = \omega_4$ | $\omega_5$ | $\omega_6 = \omega_7$ | $\omega_8$ |
|---|---|---|---|---|---|
| 0.154 | –38.292 | –16.933 | 3.261 | 1.578 | –0.191 |

From the equations (A1), (A2), (A3) and (A4) the formula for the total gear ratio of the PGS can be derived:

$$\left(i_{1,h_8}\right)_{\omega_9=0} = \frac{\omega_1}{\omega_{h_8}} = 1 - i_{1,9}^{h_8} = 1 - \frac{z_3}{z_1}\cdot\frac{z_6}{z_4}\cdot\frac{z_9}{z_7} = 1000.0 \quad \text{for} \quad \omega_9 = 0, \tag{12}$$

where the *fixed carrier transmission ratio is:*

$$i_{1,9}^{h_8} = 1 - \left(i_{1,h_8}\right)_{\omega_9=0} = \frac{z_3}{z_1}\cdot\frac{z_6}{z_4}\cdot\frac{z_9}{z_7} = -999.0\,. \tag{13}$$

3.3.2. Transmission ratios on power flow paths in subsystems of analysed PGS

According to Figure 4(a),(b), Figure 5 and Table 1 PGS consists of subsystems A, B with two DoF each and subsystem C with single DoF. Each single DoF subsystem has only one power flow path, so the transmission ratio on power flow paths of such subsystem is equal to its gear ratio. In contrast, each two DoF subsystem has two power flow paths. For this reason, for subsystems with two DoF, it is possible to determine only the transmission ratios on individual paths of the power flow, taking into account the angular velocity of the third element of each subsystem. The values of these ratios have been calculated in the Appendix D and presented in Table 5. According to the algorithm (subsubsection 2.2.1), they will be used to determine the torque acting on the sun and rim gears and carriers of each of the subsystems A, B, C and the power on individual power flow paths (Appendix D).

Preprints (www.preprints.org) | NOT PEER-REVIEWED | Posted: 3 August 2023 doi:10.20944/preprints202308.0223.v1



**Table 5.** The transmission ratios on the power flow paths in subsystems of analysed PGS.

| $\left(i_{1,h_2}\right)_{\omega_3=-16.933}$ | $\left(i_{1,3}\right)_{\omega_{h_2}=0.154}$ | $\left(i_{4,6}\right)_{\omega_{h_5}=0.154}$ | $\left(i_{h_5,6}\right)_{\omega_4=-16.933}$ | $\left(i_{7,h_8}\right)_{\omega_9=0}$ |
|---|---|---|---|---|
| 1000 | $-9.09(09)$ | −10.732 | 0.098 | 10.247 |

3.3.3. Calculations of the shaft torques of subsystems A, B, C

- Shaft torques of the two DoF subsystem A

According to Figure 4(a) and Table 3, the torque acting on the input shaft I of the PGS is given $T_I = T_1 = 10\,\mathrm{N\cdot m}$. Therefore, it was used to calculate the active and reactive torques $T_{h_2}$, $T_{h_2R}$ and $T_3$, $T_{3R}$ on the shafts of carrier $h_2$ and rim gear 3, respectively in Appendix C. Equilibrium equations (C2) and (C11) to (C13) were derived using the free body diagram based on Figure C1. The magnitudes of the calculated torques are presented in Table 6. In subsubsection 3.3.4 they will be used together with the magnitudes of angular velocities $\omega_{h_2}$ and $\omega_3$ (from Table 4) to select the appropriate system of equations to determine the two power flow paths in subsystem A.

**Table 6.** Torque magnitudes $T_{h_2}$, $T_{h_2R}$ and $T_3$, $T_{3R}$.

| $T_{h_2} = T_1\cdot\left(1-i_{1,3}^{h_2}\right)$ | $T_{h_2R} = -T_1\cdot\left(1-i_{1,3}^{h_2}\right)$ | $T_3 = T_1\cdot i_{1,3}^{h_2}$ | $T_{3R} = -T_1\cdot i_{1,3}^{h_2}$ |
|---|---|---|---|
| $100.0\,\mathrm{N\cdot m}$ | $-100.0\,\mathrm{N\cdot m}$ | $-90.0\,\mathrm{N\cdot m}$ | $90.0\,\mathrm{N\cdot m}$ |

- Shaft torques of the two DoF subsystem B

According to equation (C15) and Figure C2 the torque $T_4$ acting on the input shaft of the sun gear 4 is equal to $T_4 = -T_{3R} = -90\,\mathrm{N\cdot m}$. Therefore, it was used to calculate the active and reactive torques $T_{h_5}$, $T_{h_{5R}}$ and $T_6$, $T_{6R}$ of the carrier $h_5$ and rim gear 6 shafts, respectively. The magnitudes and vector directions of these torques were determined in Appendix C from the equilibrium equations (C16), (C25) to (C28) based on Figure C3. The magnitudes of the calculated torques are presented in Table 7. In subsubsection 3.3.4 they will be used together with the angular velocities $\omega_{h_5}$ and $\omega_6$ (from Table 6) to select the appropriate system of equations to determine the two power flow paths in subsystem B.

**Table 7.** Torque magnitudes $T_{h_5}$, $T_{h_5R}$ and $T_6$, $T_{6R}$.

| $T_{h_5} = -T_1\cdot i_{1,3}^{h_2}\cdot\left(1-i_{4,6}^{h_5}\right)$ | $T_{h_5R} = T_1\cdot i_{1,3}^{h_2}\cdot\left(1-i_{4,6}^{h_5}\right)$ | $T_6 = T_1\cdot i_{1,3}^{h_2}\cdot i_{4,6}^{h_5}$ | $T_{6R} = -T_1\cdot i_{1,3}^{h_2}\cdot i_{4,6}^{h_5}$ |
|---|---|---|---|
| $1170.0\,\mathrm{N\cdot m}$ | $-1170.0\,\mathrm{N\cdot m}$ | $1080.0\,\mathrm{N\cdot m}$ | $-1080.0\,\mathrm{N\cdot m}$ |

- Shaft torques of the single DoF subsystem C

According to equations (C29), (C30) and Figure C4, the torque acting on the shaft of the rim gear 7 is given $T_7 = -T_{6R} = 1080\,\mathrm{N\cdot m}$. Therefore, it was used to calculate the active and reactive torques $T_{h_8}$, $T_{h_8R}$ and $T_9$, $T_{9R}$ of the shafts of carrier $h_8$ and rim gear 9, respectively. Magnitudes and directions of these torques were determined in Appendix C from the equilibrium equations (C37), (C38), (C41), (C42) based on Figure C5. The magnitudes of the calculated torques are presented in Table 8. In subsubsection 3.3.4 they will be used together with the angular velocities $\omega_{h_8}$ and $\omega_9 = 0$ (from Table 4) to select the appropriate equation to determine the one power flow path in subsystem C.

Preprints (www.preprints.org) | NOT PEER-REVIEWED | Posted: 3 August 2023 doi:10.20944/preprints202308.0223.v1



**Table 8.** Torque magnitudes $T_{h_8}$, $T_{h_8R}$ and $T_9$, $T_{9R}$.

| $T_{h_8} = T_1 \cdot i_{1,3}^{h_2} \cdot i_{4,6}^{h_5} \cdot \left(1 - i_{7,9}^{h_8}\right)$ | $T_{h_8R} = -T_1 \cdot i_{1,3}^{h_2} \cdot i_{4,6}^{h_5} \cdot \left(1 - i_{7,9}^{h_8}\right)$ | $T_9 = T_1 \cdot i_{1,3}^{h_2} \cdot i_{4,6}^{h_5} \cdot i_{7,9}^{h_8}$ | $T_{9R} = -T_1 \cdot i_{1,3}^{h_2} \cdot i_{4,6}^{h_5} \cdot i_{7,9}^{h_8}$ |
|---|---|---|---|
| 11070.0 N·m | –11070.0 N·m | –9990.0 N·m | 9990.0 N·m |

3.3.4. Power flow paths in the subsystems A, B, C of the PGS

- Identification of the power flow paths in type 2(a), 2(e) or 2(f) subsystem A

In subsubsection 2.2.5 it was shown that one of the three versions of the system of equations ((6),(7)), ((8), (9)) or ((10), (11)) can be a great help in identifying active and passive shafts in series-parallel connected PGS subsystems. Each system of equations in these three versions models the subsystems of type 2(a), 2(e ) and 2(f) in order. The chosen version of the system of equations is the one that is satisfied by one of the following pairs of necessary conditions:

$$T_{3R} \cdot \omega_3 = -1523.987\,\mathrm{W} < 0 \quad \text{and} \quad T_{h_2R} \cdot \omega_{h_2} = -15,394\,\mathrm{W} < 0\,, \tag{14}$$

$$T_{3R} \cdot \omega_3 = -1523,987\,\mathrm{W} < 0 \quad \text{and} \quad T_{h_2} \cdot \omega_{h_2} = 15,394\,\mathrm{W} > 0\,, \tag{15}$$

$$T_3 \cdot \omega_3 = 1523,987\,\mathrm{W} > 0 \quad \text{and} \quad T_{h_2R} \cdot \omega_{h_2} = -15,394\,\mathrm{W} < 0\,. \tag{16}$$

It can be easily shown that the system of equations ((6), (7)) is satisfied by a pair of conditions (14). The adapted version of the selected system of equations ((6), (7)) for the new indices of subsystem A elements took the form:

$$T_1 + T_{3R} + T_{h_2R} = 0\,, \tag{17}$$

$$T_1 \cdot \omega_1 + T_{3R} \cdot \omega_3 + T_{h_2R} \cdot \omega_{h_2} = 0\,, \tag{18}$$

where adapted new indices $\alpha = 1$, $\beta = 3$ and $h = h_2$ (according to Figure 2a).

The above two equations are a mathematical model of subsystem A type 2(a), in which the input shaft of sun gear 1 is assumed to be driving ($T_1 \cdot \omega_1 = 1539.380\,\mathrm{W} > 0$), while the shafts of carrier $h_2$ and ring gear 3 are driven ($T_{3R} \cdot \omega_3 < 0$ and $T_{h_2R} \cdot \omega_{h_2} < 0$). The directions of the torques $\mathbf{T}_1$, $\mathbf{T}_{h_2R}$ and $\mathbf{T}_{3R}$ are shown in Figure 6.

Torque $T_{3R}$ must also satisfy the additional equation of energy balance in the carrier $h_2$ mobile frame of reference (19), so there is a second way to check its magnitude in addition to the free body diagram used in Appendix C (equation (C14)):

$$T_1 \cdot \left(\omega_1 - \omega_{h_2}\right) + T_{3R} \cdot \left(\omega_3 - \omega_{h_2}\right) = 0\,. \tag{19}$$

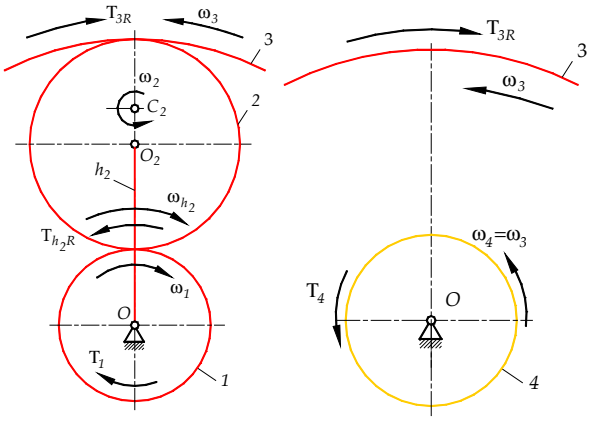


**(a)** **(b)**

Preprints (www.preprints.org) | NOT PEER-REVIEWED | Posted: 3 August 2023 doi:10.20944/preprints202308.0223.v1



**Figure 6.** Angular velocities and torques (**a**) of elements of subsystem A (**b**) of gear pair 3, 4 .

- Identification of the power flow paths in type 2(a), 2(e) or 2(f) subsystems B

A possible condition to satisfy one of the three versions of equation pairs ((6),(7)), ((8), (9)) or ((10), (11)) for the subsystem B is among the three below:

$$T_{6R} \cdot \omega_6 = -1704.094\,W < 0 \quad \text{and} \quad T_{h_5R} \cdot \omega_{h_5} = -180.107\,W < 0\,, \tag{20}$$

$$T_{6R} \cdot \omega_6 = -1704.094\,W < 0 \quad \text{and} \quad T_{h_5} \cdot \omega_{h_5} = 180.107\,W > 0\,, \tag{21}$$

$$T_6 \cdot \omega_6 = 1704,094\,W > 0 \quad \text{and} \quad T_{h_5R} \cdot \omega_{h_5} = -180.107\,W < 0\,. \tag{22}$$

The system of equations ((8), (9)) is satisfied by a pair of conditions (21), and therefore the adapted version of these equations takes the following form for subsystem B indices:

$$T_4 + T_{6R} + T_{h_5} = 0\,, \tag{23}$$

$$T_4 \cdot \omega_4 + T_{6R} \cdot \omega_6 + T_{h_5} \cdot \omega_{h_5} = 0\,, \tag{24}$$

where adapted new indices $\alpha = 4$, $\beta = 6$ and $h = h_5$ (according to Figure 2(e).

The equations (23) and (24) are a mathematical model of subsystem B type 2(e), in which the input shaft of sun gear 4 must be driving ($T_4 \cdot \omega_4 = T_3 \cdot \omega_3 = 1523,987\,W > 0$), while the shaft of rim gear 6 is driven ($T_{6R} \cdot \omega_6 < 0$), and the shaft of carrier $h_5$ is driving ($T_{h_5} \cdot \omega_{h_5} > 0$). The directions of torque vectors $\mathbf{T}_4$, $\mathbf{T}_{h_5}$ and $\mathbf{T}_{6R}$ are shown in Figure 9.

The torque $T_{6R}$ must also satisfy the additional equation of the energy balance in the mobile reference frame related to the carrier $h_5$ (25), so there is a second way to check its magnitude in addition to the free body diagram used in Appendix C (equation (C28)):

$$T_4 \cdot (\omega_4 - \omega_{h5}) + T_{6R} \cdot (\omega_6 - \omega_{h_5}) = 0\,. \tag{25}$$

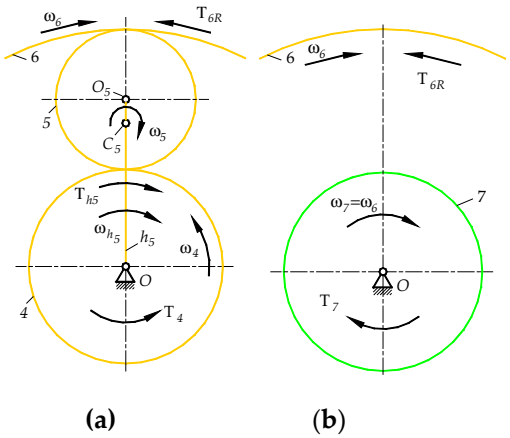


**Figure 7. A**ngular velocities and torques (**a**) of elements of subsystem B (**b**) of gear pair 6, 7.

- Identification of the power flow path in the type 1(a) subsystem C

According to Figure 3(a), Figure 4, Figure 6(a) and Table 1, the subsystem C has one DoF and is type 1(a). Therefore, it has one power flow path from the input shaft of sun gear 7 to the output shaft of carrier $h_8$ because the shaft of ring gear 9 is fixed. In this case, the governing equation can be determined directly without fitting the conditions for active and passive shafts with one of the three versions of the equations ((6),(7)), ((8), (9)) or ((10), (11)):

Preprints (www.preprints.org) | NOT PEER-REVIEWED | Posted: 3 August 2023 doi:10.20944/preprints202308.0223.v1



$$T_7 + T_{9R} + T_{h_8R} = 0, \tag{26}$$

$$T_7 \cdot \omega_7 + T_{9R} \cdot \omega_9 + T_{h_8R} \cdot \omega_{h_8} = 0, \tag{27}$$

where adapted new indices $\alpha = 7$, $\beta = 9$, $h = h_8$ (according to Figure 3(a)) and $T_7 = T_6 = -T_{6R} = 1080\ \mathrm{N \cdot m}$ (according to equations (C27) and (C30)).

The form of these equations is consistent with the assumption that in this subsystem having one DoF the shaft of sun gear 7 is driving, the shaft of carrier $h_8$ is driven, and the ring gear 9 is fixed ($\omega_9 = 0$). These assumptions correspond to the conditions, $T_7 \cdot \omega_7 = 1704.094\ \mathrm{W}$, $T_{h_8R} \cdot \omega_{h_8} < 0$ and $T_{9R} \cdot \omega_9 = 0$. The directions of the torque vectors $\mathbf{T}_{h_8R}$ and $\mathbf{T}_{9R}$ are shown in Figure 10 and Figure C5. The torque $T_{9R}$ must also satisfy the additional energy balance equation in the reference frame related to the carrier $h_8$ (28), so there is a second way to check its magnitude in addition to the free body diagram used in Appendix C (equation (C38):

$$T_7 \cdot \left(\omega_7 - \omega_{h_8}\right) + T_{9R} \cdot \left(\omega_9 - \omega_{h_8}\right) = 0. \tag{28}$$

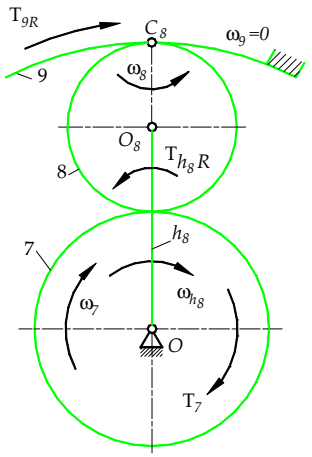


**Figure 8.** Angular velocities and torques of elements of subsystem C.

For the previously determined torques acting on the shafts of carriers $h_2$, $h_5$ and $h_8$, it is possible to calculate the total torque on the output shaft II of analysed PGS:

$$T_{IIR} = -T_{II} = T_{h_2R} + T_{h_5} + T_{h_8R} = -10000\ \mathrm{N \cdot m}. \tag{29}$$

and check the total gear ratio (for efficiency $\eta_{I,II} = 1$):

$$i_{I,II} = \frac{T_{II}}{T_I \cdot \eta_{I,II}} = \frac{10000}{10 \cdot 1} = 1000. \tag{30}$$

- Identification of the power flow path in analysed PGS (summary)

Based on equations (17), (18), (23), (24) and (28), (29) and Table 6 collective Table 9 was prepared, which presents the active and passive gears and carriers of analysed PGS, and thus the active and passive shafts of these elements.

**Table 9.** Active and reactive shafts of analysed PGS.

| Parameter | Shafts of gear or carrier No. | | | | | | | |
|---|---|---|---|---|---|---|---|---|
| | 1 | 3 | $h_2$ | 4 | 6 | $h_5$ | 7 | $h_8$ |

Preprints (www.preprints.org) | NOT PEER-REVIEWED | Posted: 3 August 2023 doi:10.20944/preprints202308.0223.v1



| $\omega_i$ | $\omega_1 > 0$ | $\omega_3 < 0$ | $\omega_{h_2} > 0$ | $\omega_4 < 0$ | $\omega_6 > 0$ | $\omega_{h_5} > 0$ | $\omega_7 > 0$ | $\omega_{h_8} > 0$ |
|---|---|---|---|---|---|---|---|---|
| $T_i$ | $T_1 > 0$ | $T_3 < 0$ | $T_{h_2} > 0$ | $T_4 < 0$ | $T_6 > 0$ | $T_{h_5} > 0$ | $T_7 > 0$ | $T_{h_8} > 0$ |
| $T_{iR}$ | $T_{1R} < 0$ | $T_{3R} > 0$ | $T_{h_2 R} < 0$ | $T_{4,R} > 0$ | $T_{6,R} < 0$ | $T_{h_5 R} < 0$ | $T_{7R} < 0$ | $T_{h_8 R} < 0$ |
| Charakter | Active | Reactive | Reactive | Active | Reactive | Active | Active | Reactive |
| Type | 2(a) | 2(a) | 2(a) | 2(e) | 2(e) | 2(e) | 1(a) | 1(a) |

3.3.5. Powers and power ratios on the shafts of subsystems A, B, C of analysed PGS

- Calculations of powers and power ratios on the shafts of subsystem A

Power calculations and power ratios in the subsystem A were made in Appendix D (equations D1 to D7). The values of the power and power ratios are presented in Table 10 and Table 11, respectively, and in Figure 9.

**Table 10.** Values of active and reactive power on the shafts of subsystem A.

| $P_1 = T_1 \cdot \omega_1$ | $P_{3R} = T_{3R} \cdot \omega_3$ | $P_{h_2 R} = T_{h_2 R} \cdot \omega_{h_2}$ |
|---|---|---|
| 1539.380 W | −1523.987 W | −15.394 W |

**Table 11.** Power ratios on the shafts of subsystem A.

| $\lvert P_{h_2 R} \rvert / P_1 \cdot 100\%$ | $\lvert P_{3R} \rvert / P_1 \cdot 100\%$ | $\left( \lvert P_{h_2 R} \rvert + \lvert P_{3R} \rvert \right) / P_1 \cdot 100\%$ |
|---|---|---|
| 1% | 99% | 100% |

Table 11 shows that only 1% of the power supplied to the subsystem A is transferred to the PGS output shaft, while the rest to the subsystem B through the shafts of rim gear 3 and sun gear 4.

- Calculations of powers and power ratios of the subsystem B

Power calculations and power ratios in the subsystem B were made in Appendix D (equations D8 to D15). The values of the power and power ratios are presented in Table 12 and Table 13, respectively, and in Figure 9.

**Table 12.** Values of active and reactive power on the shafts of subsystem B.

| $P_4 = T_4 \cdot \omega_4$ | $P_{h_5} = T_{h_5} \cdot \omega_{h_5}$ | $P_{6R} = T_{6R} \cdot \omega_6$ |
|---|---|---|
| 1523.987 W | 180.107 W | −1704.094 W |

**Table 13.** Power ratios on the shafts of subsystem B.

| $\lvert P_4 \rvert / P_1 \cdot 100\%$ | $\lvert P_{h_5} \rvert / P_1 \cdot 100\%$ | $\lvert P_{6R} \rvert / P_1 \cdot 100\%$ | $\lvert P_{6R} \rvert / \left( P_4 + P_{h_5} \right) \cdot 100\%$ |
|---|---|---|---|
| 99% | 11.7% | 110.7% | 100% |

Table 12 shows that the shafts of the sun gear 4 and the carrier $h_5$ of subsystem B are active because the powers $P_4 > 0$ and $P_5 > 0$. However, Table 13 and Table 15 show that the bearings and shafts of the ring gear 6, the sun gear 7, the planet gears 8 and the carriers $h_8$ and $h_5$ are overloaded by more than 10%. The reason is that the above-mentioned elements of the B and C subsystems form a closed loop inside which the power transmitted by the carrier $h_5$ shaft is closed. Colloquially, it is often said that this power circulates in a closed loop, but unfortunately it is not a vector.

- Calculations of powers and power ratios on the shafts of subsystem C

Preprints (www.preprints.org) | NOT PEER-REVIEWED | Posted: 3 August 2023 doi:10.20944/preprints202308.0223.v1



Power calculations and power ratios in the subsystem C were made in Appendix D (equations D16 to D23). The values of the power and power ratios are presented in Table 14 and Table 15, respectively, and in Figure 9.

**Table 14.** Values of active and reactive power on the shafts of subsystem C.

| $P_7 = T_7 \cdot \omega_7$ | $P_{h_8R} = T_{h_8R} \cdot \omega_{h_8}$ | $P_{9R} = T_9 \cdot \omega_9$ |
|---|---|---|
| 1704.094 W | −1704.094 W | 0 |

**Table 15.** Power ratios on the shafts of subsystem C.

| $P_7/P_1$ | $\lvert P_{h_8R}\rvert/P_1$ | $P_{9R}/P_1$ | $\lvert P_{h_8} + P_{h_5}\rvert/P_1$ | $\lvert P_{II}\rvert/P_1$ |
|---|---|---|---|---|
| 110.7 % | 110.7 % | 0 % | 99.0 % | 100 % |

where $P_{II} = P_{h_8} + P_{h_5} + P_{h_2} = -1539.380\,W$ (according to (D23)).

The shaft of the rim gear 9 is fixed, so the power $P_9 = 0$ (Table 14). Table 15 shows, among others, the value of the power ratio equal to $\lvert P_{II}\rvert/P_1 \cdot 100\% = 100\%$, which means that, according to the assumption, in the analysed PGS no power loss occurred.

## 4. Results

Figure 9 shows the paths and directions of the flow of power streams in the coupled serial-parallel planetary gear system without taking friction losses into account. To determine these paths, a modified classical method was used by explicitly introducing reaction moments (subsubsection 3.3.4 and Table 9). The calculations showed that the analyzed PGS is coupled not only structurally through two closed circuits, but also dynamically. Namely, in the second circuit there is a phenomenon of power circulation, because the shaft of carrier $h_5$ is active in contrast to the shafts of carriers $h_2$ and $h_8$, which are passive. Through the shaft of carrier $h_5$, the power is transmitted to the inside of the second PGS circuit according to the calculation results (D9) and (D13) presented in Table 15, which increased the power ratio to 110.7% according to the calculation results (D14), (D19) and (D20). Through the shafts of carriers $h_2$ and $h_8$, the power is transmitted to the output shaft II PGS, i.e. outside according to the calculation results (D3) and D20). As a result of the power circulation, the meshing of the gears 5-6, 7-8, 8-9 and the adjacent rolling bearings are overloaded. The output power, despite the power circulation in a closed circuit, reached 100% of the input power.

Preprints (www.preprints.org) | NOT PEER-REVIEWED | Posted: 3 August 2023 doi:10.20944/preprints202308.0223.v1



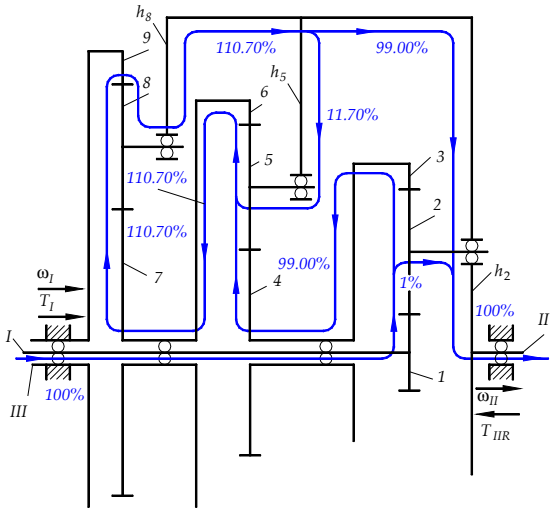


**Figure 9.** Directions of power streams flow and power ratios in the coupled PGS.

## 5. Conclusions

In this paper, which is the first part of a three-part study, a systematic methodology of determining the paths and directions of power flow in coupled serial-parallel PGS has been presented. These single degree of freedom PGSs consisted of three 2KH type subsystems and two closed circuits. The aim of developing the three parts of the study was:

1) comparison of power flow paths and directions without taking into account power losses in two structurally similar PGSs, the first of which turned out to be structurally coupled (with a closed circuit) and dynamically coupled (with the power circulation phenomenon) during the analysis carried out in Part I, while the second PGS analyzed in part II - only structurally coupled without power circulation,

2) comparison of power flow paths and directions, taking into account power losses in gear meshing, and determination of power ratios and efficiency of these two PGSs (in Part III).

The algorithm of the method was as follows (assuming that the geometric parameters of PGS are already given):

1) checking the PGS mobility, dividing the PGS structure into blocks (subsystems) and closed circuits, determining the fixed carrier transmission ratio of individual subsystems,

2) determination of the magnitudes of angular velocities of gears and carriers as well as gear ratios of individual subsystems and PGS using the Willis relationship,

3) determining the magnitudes of active and reactive torques, as well as tangential and radial forces, using the free body diagram, necessary to calculate the active or reactive powers transmitted by the shafts of individual subsystems,

4) determination of paths with power flow directions by defining the role of individual subsystem shafts (active shafts - supplying power to the subsystem, passive shafts discharging power from the subsystem) - an original method using the concepts of active and reactive torques, as well as active and reactive powers,

5) calculation of power values and power ratios as a check of the algorithm.

**Author Contributions:** Conceptualization, J.D. and T.K.; methodology, J.D. and T.K.; software, K.S.; formal analysis, T.K.; writing—original draft preparation, J.D. and T.K.; writing—review and editing, J.D.; visualization, J.D., J.R. and K.S.; funding acquisition, J.D. All authors have read and agreed to the published version of the manuscript.".

**Funding:** This research received no external funding.

**Conflicts of Interest:** "The authors declare no conflict of interest.".

## Appendix A

Preprints (www.preprints.org) | NOT PEER-REVIEWED | Posted: 3 August 2023 doi:10.20944/preprints202308.0223.v1



*A.1. Willis formulas for subsystems A, B, C and PGS*

- Equation for subsystem A (Figure B1):

$$i_{1,3}^{h_2} = \frac{\omega_1 - \omega_{h_2}}{\omega_3 - \omega_{h_2}}, \quad \text{(A1)}$$

where: $i_{1,3}^{h_2} = z_3/z_1 = -9$, $\omega_1 = 153.938\,\text{rad/s}$, $\omega_3 = \omega_4$, $\omega_{h_2} = \omega_{II}$ (Figure 5(c), Table 2).

- Equation for subsystem B (Figure B2):

$$i_{4,6}^{h_5} = \frac{\omega_4 - \omega_{h_5}}{\omega_6 - \omega_{h_5}}, \quad \text{(A2)}$$

where: $i_{4,6}^{h_5} = z_6/z_4 = -12$, $\omega_6 = \omega_7$, $\omega_{h_5} = \omega_{II} = \omega_{h_2}$ (Figure 5(b), Table 2).

- Equation for subsystem C (Figure B3):

$$i_{7,9}^{h_8} = \frac{\omega_7 - \omega_{h_8}}{\omega_9 - \omega_{h_8}}, \quad \text{(A3)}$$

where: $i_{7,9}^{h_8} = z_9/z_7 = -9.25$, $\omega_{h_2} = \omega_{h_5} = \omega_{h_8} = \omega_{II}$, $\omega_9 = 0$ (Figure 5(a), Table 2).

- Equation for PGS (Figure 4(a), Figure 5):

$$i_{1,9}^{h_8} = \frac{\omega_1 - \omega_{h_8}}{\omega_9 - \omega_{h_8}}, \quad \text{(A4)}$$

*A.2. Willis formulas for sun gear and planet gear pairs*

- Equation for the sun gear 1 and the planet gear 2:

$$i_{1,2}^{h_2} = \frac{\omega_1 - \omega_{h_2}}{\omega_2 - \omega_{h_2}}, \quad \text{(A5)}$$

where: $i_{1,2}^{h_2} = -z_2/z_1 = -4$ (Figure 5(c)).

- Equation for the sun gear 4 and the planet gear 5:

$$i_{4,5}^{h_5} = \frac{\omega_4 - \omega_{h_5}}{\omega_5 - \omega_{h_5}}, \quad \text{(A6)}$$

where: $i_{4,5}^{h_5} = -z_5/z_4 = -5.5$ (Figure 5(b)).

- Equation for the sun gear 7 and the planet gear 8:

$$i_{7,8}^{h_8} = \frac{\omega_7 - \omega_{h_8}}{\omega_8 - \omega_{h_8}}, \quad \text{(A7)}$$

where: $i_{7,8}^{h_8} = -z_8/z_7 - 4.125$ (Figure 5(a)).

*A.3. Calculations of angular velocities of gears and carriers of PGS*

- Angular velocities of the carriers $h_2$, $h_5$ and $h_8$:

Preprints (www.preprints.org) | NOT PEER-REVIEWED | Posted: 3 August 2023 doi:10.20944/preprints202308.0223.v1



$$\omega_{h_2} = \omega_{h_5} = \omega_{h_8} = \omega_{II} = \frac{\omega_1}{i^9_{1,h_8}} = 0.154 \text{ rad/s}. \quad \text{(A8)}$$

- Angular velocities of the rim gear 3 and the sun gear 4:

$$\omega_3 = \left(\omega_1 - \omega_{h_2}\right) \cdot \frac{z_1}{z_3} + \omega_{h_2} = -16.933 \text{ rad/s} \quad \text{(A9)}$$

or

$$\omega_4 = \omega_{h_5} \cdot \left(1 - \frac{z_9}{z_7} \cdot \frac{z_6}{z_4}\right) = \frac{\omega_1}{i^9_{1h_5}} \cdot \left(1 - \frac{z_9}{z_7} \cdot \frac{z_6}{z_4}\right) = -16.933 \text{ rad/s}. \quad \text{(A10)}$$

- Angular velocities of the rim gear 6 and the sun gear 7:

$$\omega_6 = \omega_7 = \left(\omega_1 - \omega_{h_2}\right) \cdot \frac{z_1}{z_3} \cdot \frac{z_4}{z_6} + \omega_{h_2} = 1.578 \text{ rad/s} \quad \text{(A11)}$$

or

$$\omega_7 = \omega_{h_8} \cdot \left(1 - \frac{z_9}{z_7}\right) \Rightarrow \omega_7 = \frac{\omega_1}{i^9_{1h_8}} \cdot \left(1 - \frac{z_9}{z_7}\right) = \omega_6 = 1.578 \text{ rad/s}. \quad \text{(A12)}$$

- Angular velocity of the planet gear 2:

$$\omega_2 = -\frac{z_1}{z_2} \cdot \omega_1 + \omega_{h_2} \cdot \left(1 + \frac{z_1}{z_2}\right) = -38.292 \text{ rad/s}. \quad \text{(A13)}$$

- Angular velocity of the planet gear 5:

$$\omega_5 = -\frac{z_4}{z_5} \cdot \omega_4 + \omega_{h_5} \cdot \left(1 + \frac{z_4}{z_5}\right) = 3.261 \text{ rad/s}, \quad \text{(A14)}$$

- Angular velocity of the planet gear 8:

$$\omega_8 = -\frac{z_7}{z_8} \cdot \omega_7 + \omega_{h_8} \cdot \left(1 + \frac{z_7}{z_8}\right) = -0.191 \text{ rad/s}. \quad \text{(A15)}$$

## Appendix B

*B.1. Calculation of tangential velocities of the gears of PGS*

- Tangential velocities $v_{1,2}$, $v_{4,5}$, $v_{7,8}$ of the sun gears 1, 4, 7 respectively at the points of contact with the planet gears 2, 5, 8 are determined from the following formulas (according to Figure B1, Figure B2 and Figure B3):

$$v_{i,i+1} = \omega_i \cdot \frac{d_i}{2}, \quad \text{(B1)}$$

where $i = 1, 4, 7$.

- Tangential velocities $v_{3,2}$, $v_{6,5}$, $v_{9,8}$ of rim gears 3, 6, 9 respectively at the points of contact with the planet gears 2, 5, 8 (according to Figure B1, Figure B2 and Figure B3:

$$v_{i,i-1} = \omega_i \cdot \frac{|d_i|}{2}, \quad \text{(B2)}$$

where $i = 3, 6, 9$.

Preprints (www.preprints.org) | NOT PEER-REVIEWED | Posted: 3 August 2023 doi:10.20944/preprints202308.0223.v1



- Assumption that the tangential velocities of the planet gears $v_{2,1}$, $v_{2,3}$, $v_{5,4}$, $v_{5,6}$, $v_{8,7}$, $v_{8,9}$ are equal to the respective velocities of the sun and rim gears at their points of contact (according to Figure B1, Figure B2 and Figure B3):

$$v_{2,1} = v_{1,2}, \quad v_{2,3} = v_{3,2}, \quad v_{5,4} = v_{4,5}, \quad v_{5,6} = v_{6,5}, \quad v_{8,7} = v_{7,8}, \quad v_{8,9} = v_{9,8}.$$

The calculated magnitudes of these velocities are given in Table B1.

**Table B1.** Calculated magnitudes of tangential velocities in $m/s$.

| $v_{2,1} = v_{1,2}$ | $v_{2,3} = v_{3,2}$ | $v_{5,4} = v_{4,5}$ | $v_{5,6} = v_{6,5}$ | $v_{8,7} = v_{7,8}$ | $v_{8,9} = v_{9,8}$ |
|---|---|---|---|---|---|
| 1.385 | -1.372 | -0,229 | 0.256 | 0.047 | 0 |

*B.2. Determination of instantaneous centre of zero velocity* $C_2$ *and velocities of the carrier* $h_2$

- The coordinate $x_2$ of the instantaneous centre of zero velocity $C_2$ of the planet gear 2 (Figure B1(a)):

$$\frac{v_{2,1}}{x_2} = \frac{-v_{2,3}}{d_2 - x_2} \quad \Rightarrow \quad x_2 = \frac{v_{2,1} \cdot d_2}{v_{2,1} - v_{2,3}} = 0.036 \text{ m}. \tag{B3}$$

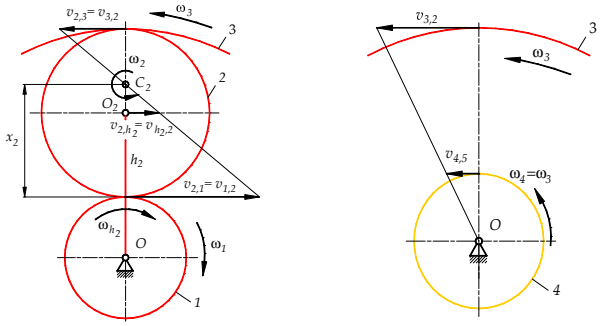


(**a**) (**b**)

**Figure B1.** Angular and tangential velocities **(a)** of the elements of subsystem A **(b)** of the pair of gears 3, 4.

- Angular velocity $\omega_2$ of the planet gear 2 (check (A13)):

$$\omega_2 = -\frac{v_{2,1}}{x_2} = \frac{v_{2,3}}{d_2 - x_2} = -38.292 \text{ rad/s}. \tag{B4}$$

- Tangential velocities $v_{2,h_2}$ and $v_{h_2,2}$ of the centre $O_2$ of the planet gear 2 and the carrier $h_2$, respectively (Figure B1(a)):

$$v_{2,h_2} = v_{h_2,2} = -\omega_2 \cdot \left( x_2 - \frac{d_2}{2} \right) = 0.007 \text{ m/s}. \tag{B5}$$

- Angular velocities $\omega_{h_2}$ of the carrier $h_2$ (Figure B1(a)):

$$v_{h_2,2} = \omega_{h_2} \cdot \frac{d_1 + d_2}{2} \quad \Rightarrow \quad \omega_{h_2} = v_{h_2,2} \cdot 2/(d_1 + d_2) = 0.154 \text{ rad/s}. \tag{B6}$$

- Tangential velocity $v_{4,5}$ of the sun gear 4 at the point of contact with the planet gears 5 (Figure B1(b)):

$$\omega_4 = \omega_3 \quad \Rightarrow \quad v_{4,5}/(d_4/2) = v_{3,2}/(|d_3|/2) \quad \Rightarrow \quad v_{4,5} = v_{3,2} \cdot d_4/|d_3| = -0.229 \text{ m/s}. \tag{B7}$$

Preprints (www.preprints.org) | NOT PEER-REVIEWED | Posted: 3 August 2023 doi:10.20944/preprints202308.0223.v1



*B.3. Determination of instantaneous centre of zero velocity* $C_5$ *and velocities of the carrier* $h_5$

- The coordinate $x_5$ of the instantaneous centre of zero velocity $C_5$ of the planet gear 5 (Figure B2(a)):

$$\frac{-v_{5,4}}{x_5}=\frac{v_{5,6}}{d_5-x_5} \quad \Rightarrow \quad x_5=\frac{-v_{5,4}\cdot d_5}{-v_{5,4}+v_{5,6}}=0.070 \text{ m}. \tag{B8}$$

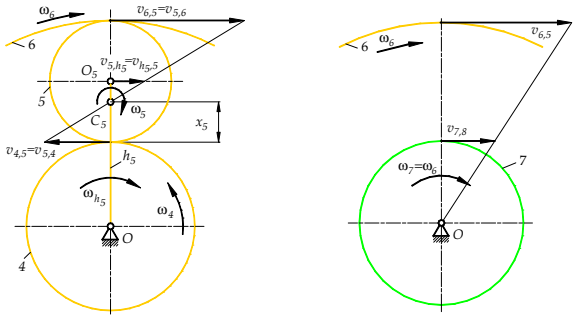


**Figure B2.** Angular and tangential velocities **(a)** of the elements of subsystem B **(b)** of the pair of gears 6, 7.

- Angular velocity $\omega_5$ of the planet gear 5 (check (A14)):

$$\omega_5=\frac{-v_{5,4}}{x_5}=\frac{v_{5,6}}{d_5-x_5}=3.261 \text{ rad/s}, \tag{B9}$$

- Tangential velocities $v_{5,h_5}$ and $v_{h_5,5}$ of the centre $O_5$ of the planet gear 5 and the carrier $h_5$, respectively (Figure B2(a)):

$$v_{5,h_5}=v_{h_5,5}=-\omega_5\cdot\left(\frac{d_5}{2}-x_5\right)=0.014\,\text{m/s}. \tag{B10}$$

- Angular velocity $\omega_{h_5}$ of the carrier $h_5$ (Figure B2(a)):

$$v_{h_5,5}=\omega_{h_5}\cdot\frac{d_4+d_5}{2} \quad \Rightarrow \quad \omega_{h_5}=v_{h_5,5}\cdot 2/(d_4+d_5)=0.154 \text{ rad/s}. \tag{B11}$$

- Tangential velocity $v_{7,8}$ of the sun gear 7 at the point of contact with the planet gears 8 (Figure B2(b)):

$$\omega_7=\omega_6 \quad \Rightarrow \quad v_{7,8}/(d_7/2)=v_{6,5}/(|d_6|/2) \quad \Rightarrow \quad v_{7,8}=v_{6,5}\cdot d_7/|d_6|=0{,}047\,\text{m/s}. \tag{B12}$$

*B.4. Determination of instantaneous centre of zero velocity* $C_8$ *and velocities of the carrier* $h_8$

- The coordinate of the instantaneous centre of zero velocity $C_8$ of the planet gear 8 (Figure B3):

Instantaneous centre of zero velocity of the gear 8 is at the point $C_8$ of contact with the stationary ring gear 8, because $\omega_9=0$ (Figure B3). Thus tangential velocities $v_{8,9}$ and $v_{9,8}$ are equal $v_{8,9}=v_{9,8}=0$.

Preprints (www.preprints.org) | NOT PEER-REVIEWED | Posted: 3 August 2023 doi:10.20944/preprints202308.0223.v1



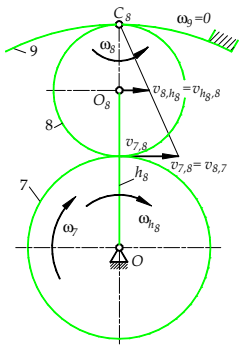


**Figure B3.** Angular and tangential velocities of subsystem C.

- Angular velocity $\omega_8$ of the planet gear 8 (check (A15)):

$$\omega_8 = -\frac{v_{8,7}}{d_8} = -0.191 \text{ rad/s}, \qquad \text{(B13)}$$

where: $v_{8,7} = v_{7,8} = 0.047 \text{ m/s}$ (according to (B12)).

- Magnitude of velocities $v_{8,h_8}$ and $v_{h_8,8}$, respectively, of the center $O_8$ of the planet gear 8 and the carrier $h_8$ (Figure B3):

$$v_{8,h_8} = v_{h_8,8} = -\omega_8 \cdot \frac{d_8}{2} = 0.024 \text{ m/s}. \qquad \text{(B14)}$$

- Angular velocity $\omega_{h_8}$ of the carrier $h_8$ (Figure B3):

$$v_{h_8,8} = \omega_{h_8} \cdot \frac{d_7 + d_8}{2} \quad \Rightarrow \quad \omega_{h_8} = v_{h_8,8} \cdot 2/(d_7 + d_8) = 0.154 \text{ rad/s}. \qquad \text{(B15)}$$

**Table B2.** Velocity magnitudes of the centres of planet gears 2, 5, 8 and the carriers $h_2$, $h_5$ and $h_8$ in m/s.

| $v_{2,h_2} = v_{h_2,2}$ | $v_{5,h_5} = v_{h_5,5}$ | $v_{8,h_8} = v_{h_8,8}$ |
|---|---|---|
| 0.007 | 0.014 | 0.024 |

## Appendix C

*C.1. Calculation of torques, tangential and radial forces acting on gears 1, 2, 3 and carrier* $h_2$

- The reaction torque $T_{1R}$ balancing the given active torque $T_1$ according to Table 2 and Figure C1(a):

$$T_1 + T_{1R} = 0 \quad \Rightarrow \quad T_{1R} = -T_1 = -10 \text{ N} \cdot \text{m}. \qquad \text{(C1)}$$

- The tangential force $F_{t2,1}$ exerted by the planet gear 2 on the sun gear 1 (Figure C1(a)):

$$T_{1R} = s_2 \cdot F_{t2,1} \cdot \frac{d_1}{2} \quad \Rightarrow \quad F_{t2,1} = \frac{2 \cdot T_{1R}}{s_2 \cdot d_1} = -370.370 \text{ N}. \qquad \text{(C2)}$$

- The radial force $F_{r2,1}$ exerted by the planet gear 2 on sun gear 1:

$$F_{r2,1} = \left|F_{t2,1}\right| \cdot \tan\alpha = 134.804 \text{ N}, \qquad \text{(C3)}$$

where pressure angle $\alpha = 20°$.

Preprints (www.preprints.org) | NOT PEER-REVIEWED | Posted: 3 August 2023 doi:10.20944/preprints202308.0223.v1



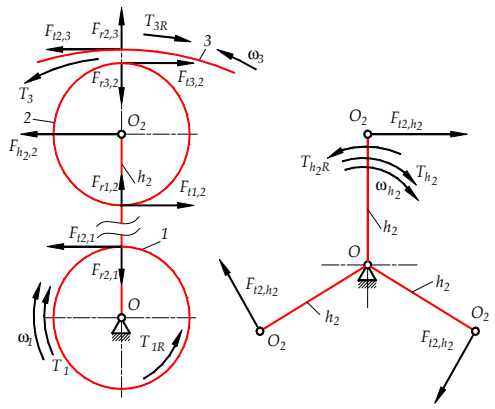


(**a**) (**b**)

**Figure C1.** Free body diagrams of the subsystem A elements: (a) gears 1, 2, 3, (b) carrier $h_2$.

- The tangential force $F_{t1,2}$ exerted by the sun gear 1 on the planet gear 2:

$$T_1 = s_2 \cdot F_{t1,2} \cdot \frac{d_1}{2} \quad \Rightarrow \quad F_{t1,2} = \frac{2 \cdot T_1}{s_2 \cdot d_1} = -F_{t2,1} = 370.370 \text{ N}. \tag{C4}$$

- The radial force $F_{r1,2}$ exerted by the sun gear 1 on the planet gear 2:

$$F_{r1,2} = \left|F_{t1,2}\right| \cdot \tan\alpha = 134.804 \text{ N}. \tag{C5}$$

- The tangential force $F_{t3,2}$ exerted by the ring gear 3 on the planet gear 2:

$$F_{t1,2} \cdot \frac{d_2}{2} - F_{t3,2} \cdot \frac{d_2}{2} = 0 \quad \Rightarrow \quad F_{t3,2} = F_{t1,2} = 370.370 \text{ N}. \tag{C6}$$

- The tangential force $F_{t2,3}$ exerted by the planet gear 2 on the ring gear 3:

$$F_{t2,3} = -F_{t3,2} = -F_{t1,2} = -370.370 \text{ N}. \tag{C7}$$

- The radial forces $F_{r2,3}$ and $F_{r3,2}$ exerted respectively by the planet gear 2 on the ring gear 3 and vice versa by the ring gear 3 on the planet gear 2:

$$F_{r2,3} = F_{r3,2} = F_{r1,2} = 134.804 \text{ N}. \tag{C8}$$

- The force $F_{h_2,2}$ exerted by the carrier $h_2$ on the center of planet gear 2 (Figure C1(b)):

$$F_{h_2,2} + F_{t1,2} + F_{t3,2} = 0 \quad \Rightarrow \quad F_{h_2,2} = -\frac{4 \cdot T_1}{s_2 \cdot d_1} = -740.741 \text{ N}. \tag{C9}$$

- The tangential force $F_{t2,h_2}$ exerted by the center of planet gear 2 on the carrier $h_2$:

$$F_{t2,h_2} = -F_{h_2,2} = \frac{4 \cdot T_1}{s_2 \cdot d_1} = 740.741 \text{ N}. \tag{C10}$$

- The active torque $T_{h_2}$ transmitted to the shaft of the working machine II through the shaft of carrier $h_2$:

$$T_{h_2} = F_{t2,h_2} \cdot s_2 \cdot \frac{d_1 + d_2}{2} = \frac{2 \cdot T_1 \cdot (z_1 + z_2)}{z_1} = 2 \cdot T_1 \cdot \left(1 - i_{1,2}^{h_2}\right) = 100 \text{ N} \cdot \text{m}. \tag{C11}$$

Preprints (www.preprints.org) | NOT PEER-REVIEWED | Posted: 3 August 2023 doi:10.20944/preprints202308.0223.v1



- The reaction torque $T_{h_2R}$ (generated by the resistance of the working machine) balancing the active torque $T_{h_2}$:

$$T_{h_2R} = F_{th_2,2} \cdot s_2 \cdot \frac{d_1 + d_2}{2} = -2 \cdot T_1 \cdot \left(1 - i_{1,2}^{h_2}\right) = -100 \text{ N} \cdot \text{m} . \quad \text{(C12)}$$

- The active torque $T_3$ transmitted to the shaft of sun gear 4 through the shaft of ring gear 3):

$$T_3 = \frac{F_{t2,3} \cdot s_2 \cdot |d_3|}{2} = -\frac{T_1 \cdot |z_3|}{z_1} = \frac{T_1 \cdot z_3}{z_1} = T_1 \cdot i_{1,3}^{h_2} = -90 \text{ N} \cdot \text{m} . \quad \text{(C13)}$$

- The reaction torque $T_{3R}$ (generated by the resistance of subsystem B) balancing the active torque $T_3$:

$$T_{3R} = \frac{F_{t3,2} \cdot s_2 \cdot |d_3|}{2} = -\frac{T_1 \cdot z_3}{z_1} = -T_1 \cdot i_{1,3}^{h_2} = 90 \text{ N} \cdot \text{m} . \quad \text{(C14)}$$

*C.2. Calculation of torques, tangential and radial forces acting on gears 4, 5, 6 and carrier* $h_5$

- The active torque $T_4$ driving the shaft of sun gear 4 according to Figures C1(a) and C2:

$$T_4 = -T_{3R} \quad \Rightarrow \quad T_4 = -T_1 \cdot i_{1,3}^{h_2} = -90 \text{ N} \cdot \text{m} . \quad \text{(C15)}$$

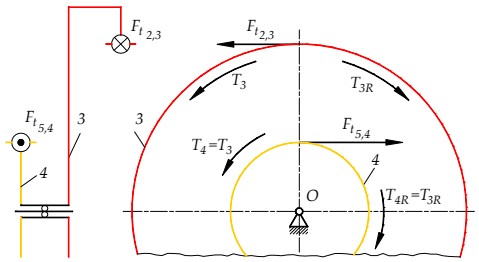


**Figure C2.** Balance of active and reaction torques acting on ring gear 3 and sun gear 4.

- The reaction torque $T_{4R}$ balancing the active torque $T_4$:

$$T_{4R} + T_4 = 0 \quad \Rightarrow \quad T_{4R} = -T_4 = -T_1 \cdot i_{1,3}^{h_2} = 90 \text{ N} \cdot \text{m} . \quad \text{(C16)}$$

- The tangential force $F_{t5,4}$ exerted by the planet gear 5 on the sun gear 4 (Figure C3(a)):

$$T_{4R} = F_{t5,4} \cdot s_5 \cdot \frac{d_4}{2} \quad \Rightarrow \quad F_{t5,4} = \frac{2 \cdot T_{4R}}{s_5 \cdot d_4} = \frac{2 \cdot T_1 \cdot |z_3|}{s_5 \cdot d_4 \cdot z_1} = -\frac{2 \cdot T_1}{s_5 \cdot d_4} \cdot i_{1,3}^{h_2} = 2222.222 \text{ N} . \quad \text{(C17)}$$

- The tangential force $F_{t4,5}$ exerted by the sun gear 4 on the planet gear 5:

$$T_4 = F_{t4,5} \cdot s_5 \cdot \frac{d_4}{2} \quad \Rightarrow \quad F_{t4,5} = -F_{t5,4} = \frac{2 \cdot T_4}{s_5 \cdot d_4} = \frac{2 \cdot T_1}{s_5 \cdot d_4} \cdot i_{1,3}^{h_2} = -2222.222 \text{ N} . \quad \text{(C18)}$$

Preprints (www.preprints.org) | NOT PEER-REVIEWED | Posted: 3 August 2023 doi:10.20944/preprints202308.0223.v1



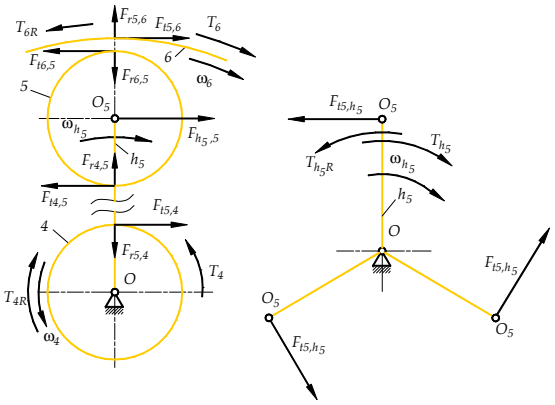


**(a)** **(b)**

**Figure C3.** Free body diagrams of the subsystem B elements: (a) gears 4, 5, 6, (b) carrier $h_5$.

- The radial forces $F_{r5,4}$ and $F_{r4,5}$ exerted respectively by the planet gear 5 on the sun gear 4 and vice versa by the sun gear 4 on the planet gear 5 (Figure C3(a)):

$$F_{r5,4} = F_{r4,5} = \left|F_{t5,4}\right| \cdot \tan\alpha = 808.823 \text{ N}. \tag{C19}$$

- The tangential force $F_{t6,5}$ exerted by the ring gear 6 on the planet gear 5:

$$F_{t4,5} \cdot \frac{d_5}{2} - F_{t6,5} \cdot \frac{d_5}{2} = 0 \quad \Rightarrow \quad F_{t6,5} = F_{t4,5} = \frac{2 \cdot T_1}{s_5 \cdot d_4} \cdot i_{1,3}^{h_2} = -2222.222 \text{ N}. \tag{C20}$$

- The tangential force $F_{t5,6}$ exerted by the planet gear 5 on the ring gear 6:

$$F_{t5,6} + F_{t6,5} = 0 \quad \Rightarrow \quad F_{t5,6} = -F_{t6,5} = -\frac{2 \cdot T_1}{s_5 \cdot d_4} \cdot i_{1,3}^{h_2} = 2222.222 \text{ N}. \tag{C21}$$

- The radial forces $F_{r5,6}$ and $F_{r6,5}$ exerted respectively by the planet gear 5 on the ring gear 6 and vice versa by the ring gear 6 on the planet gear 5 (Figure C3(a)):

$$F_{r5,6} = F_{r6,5} = \left|F_{t5,6}\right| \cdot \tan\alpha = 808.823 \text{ N}. \tag{C22}$$

- The force $F_{h_5,5}$ exerted by the carrier $h_5$ on the center of planet gear 5 (Figure C3(b)):

$$F_{h_5,5} + F_{t4,5} + F_{t6,5} = 0 \quad \Rightarrow \quad F_{h_5,5} = -F_{t4,5} - F_{t6,5} = -\frac{4 \cdot T_1}{s_5 \cdot d_4} \cdot i_{1,3}^{h_2} = 4444.444 \text{ N}. \tag{C23}$$

- The tangential force $F_{t5,h_5}$ exerted by the center of planet gear 5 on the carrier $h_5$:

$$F_{t5,h_5} + F_{h_5,5} = 0 \quad \Rightarrow \quad F_{t5,h_5} = -F_{h_5,5} = \frac{4 \cdot T_1}{s_5 \cdot d_4} \cdot i_{1,3}^{h_2} = -4444.444 \text{ N}. \tag{C24}$$

- The active torque $T_{h_5}$ driving the shaft of carrier $h_5$ and carrier $h_5$ according to Figure C3(b):

$$T_{h_5} = F_{h_5,5} \cdot s_5 \cdot \frac{d_4 + d_5}{2} = -\frac{2 \cdot T_1 \cdot (z_4 + z_5) \cdot i_{1,3}^{h_2}}{z_4} = -2 \cdot T_1 \cdot \left(1 - i_{4,5}^{h_5}\right) \cdot i_{1,3}^{h_2} = 1170 \text{ N} \cdot \text{m}. \tag{C25}$$

- The reaction torque $T_{h_5R}$ balancing the active torque $T_{h_5}$:

Preprints (www.preprints.org) | NOT PEER-REVIEWED | Posted: 3 August 2023 doi:10.20944/preprints202308.0223.v1



$$T_{h_5R} = F_{t5,h_5} \cdot s_5 \cdot \frac{d_4 + d_5}{2} = 2 \cdot T_1 \cdot \left(1 - i_{4,5}^{h_5}\right) \cdot i_{1,3}^{h_2} = -1170 \text{ N} \cdot \text{m} . \quad \text{(C26)}$$

- The active torque $T_6$ driving the shaft of sun gear 7 through the shaft of ring gear 6 (Figure C4):

$$T_6 = \frac{F_{t5,6} \cdot s_5 \cdot |d_6|}{2} = -\frac{T_1 \cdot i_{1,3}^{h_2} \cdot |z_6|}{z_4} = T_1 \cdot i_{1,3}^{h_2} \cdot i_{4,6}^{h_5} = 1080 \text{ N} \cdot \text{m} . \quad \text{(C27)}$$

- The reaction torque $T_{6R}$ balancing the active torque $T_6$:

$$T_{6R} = \frac{F_{t6,5} \cdot s_5 \cdot |d_6|}{2} \quad \Rightarrow \quad T_{6R} = -T_6 = -T_1 \cdot i_{1,3}^{h_2} \cdot i_{4,6}^{h_5} = -1080 \text{ N} \cdot \text{m} . \quad \text{(C28)}$$

*C.3. Calculation of torques, tangential and radial loads acting on gears 7,8, 9 and carrier* $h_8$

- The reaction torque $T_{7R}$ balancing the active torque $T_6$ (Figure C4):

$$T_6 + T_{7R} = 0 \quad \Rightarrow \quad T_{7R} = -T_6 = T_{6R} = -T_1 \cdot i_{1,3}^{h_2} \cdot i_{4,6}^{h_5} = -1080 \text{ N} \cdot \text{m} . \quad \text{(C29)}$$

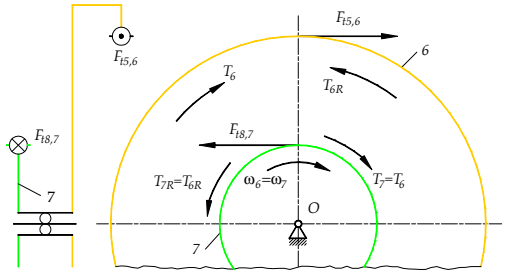


**Figure C4.** Balance of active and reaction torques acting on ring gear 6 and sun gear 7.

- The active torque $T_7$ driving the shaft of sun gear 7 (Figure C4):

$$T_7 = T_6 = 0 \quad \Rightarrow \quad T_7 = -T_{7R} = T_6 = T_1 \cdot i_{1,3}^{h_2} \cdot i_{4,6}^{h_5} = 1080 \text{ N} \cdot \text{m} . \quad \text{(C30)}$$

- The tangential force $F_{t8,7}$ exerted by the planet gear 8 on the sun gear 7 according to Figure C5(a):

$$T_{7R} = F_{t8,7} \cdot s_8 \cdot \frac{d_7}{2} \quad \Rightarrow \quad F_{t8,7} = \frac{2 \cdot T_{7R}}{s_8 \cdot d_7} = -\frac{2 \cdot T_1 \cdot i_{1,3}^{h_2} \cdot i_{4,6}^{h_5}}{s_8 \cdot d_7} = -12000 \text{ N} . \quad \text{(C31)}$$

- The tangential force $F_{t7,8}$ exerted by the sun gear 7 on the planet gear 8:

$$T_7 = F_{t7,8} \cdot s_8 \cdot \frac{d_7}{2} \quad \Rightarrow \quad F_{t7,8} = \frac{2 \cdot T_7}{s_8 \cdot d_7} = \frac{2 \cdot T_1 \cdot i_{1,3}^{h_2} \cdot i_{4,6}^{h_5}}{s_8 \cdot d_7} = 12000 \text{ N} . \quad \text{(C32)}$$

- The radial forces $F_{r8,7}$ and $F_{r7,8}$ exerted respectively by the planet gear 8 on the sun gear 7 and vice versa by the sun gear 7 on the planet gear 8 (Figure C5(a)):

$$F_{r8,7} = F_{r7,8} = \left|F_{t8,7}\right| \cdot \tan\alpha = 4367.643 \text{ N} . \quad \text{(C33)}$$

- The tangential force $F_{t9,8}$ exerted by the ring gear 9 on the planet gear 8:

$$F_{t7,8} \cdot \frac{d_8}{2} - F_{t9,8} \cdot \frac{d_8}{2} = 0 \quad \Rightarrow \quad F_{t9,8} = F_{t7,8} = \frac{2 \cdot T_1 \cdot i_{1,3}^{h_2} \cdot i_{4,6}^{h_5}}{s_8 \cdot d_7} = 12000 \text{ N} . \quad \text{(C34)}$$

Preprints (www.preprints.org) | NOT PEER-REVIEWED | Posted: 3 August 2023 doi:10.20944/preprints202308.0223.v1



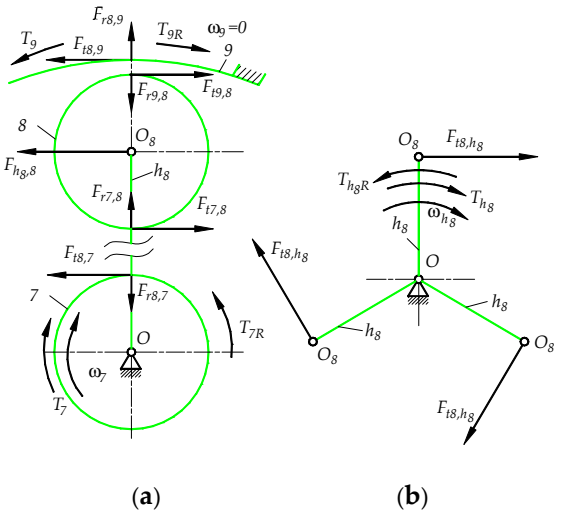


(**a**) (**b**)

**Figure C5.** Free body diagrams of the subsystem C elements: (**a**) gears 7 8, 9, (**b**) carriers $h_8$.

- The tangential force $F_{t8,9}$ exerted by the planet gear 8 on the ring gear 9:

$$F_{t8,9}+F_{t9,8}=0 \quad \Rightarrow \quad F_{t8,9}=-F_{t9,8}=-\frac{2\cdot T_1\cdot i_{1,3}^{h_2}\cdot i_{4,6}^{h_5}}{s_8\cdot d_7}=-12000\ \text{N}. \tag{C35}$$

- The radial forces $F_{r9,8}$ and $F_{r8,9}$ exerted respectively by the ring gear 9 on the planet gear 8 and vice versa by the planet gear 8 on the ring gear 9 (Figure C5(a)):

$$F_{r9,8}=F_{r8,9}=\left|F_{t9,8}\right|\cdot\tan\alpha=4367.643\ \text{N}. \tag{C36}$$

- The active torque $T_9$ loading the fixed ring gear 9:

$$T_9=\frac{F_{t8,9}\cdot s_8\cdot\left|d_9\right|}{2}=-\frac{T_1\cdot i_{1,3}^{h_2}\cdot i_{4,6}^{h_5}\cdot\left|z_9\right|}{z_7}=T_1\cdot i_{1,3}^{h_2}\cdot i_{4,6}^{h_5}\cdot i_{7,9}^{h_8}=-9990\ \text{N}\cdot\text{m}. \tag{C37}$$

- The reaction torque $T_{9R}$ balancing the active torque $T_9$:

$$T_{9R}=-T_9=\frac{F_{t9,8}\cdot s_8\cdot\left|d_9\right|}{2}=-T_1\cdot i_{1,3}^{h_2}\cdot i_{4,6}^{h_5}\cdot i_{7,9}^{h_8}=9990\ \text{N}\cdot\text{m}. \tag{C38}$$

- The force $F_{h_8,8}$ exerted by the carrier $h_8$ on the center of planet gear 8 (Figure C5(a)):

$$F_{h_8,8}+F_{t7,8}+F_{t9,8}=0 \quad \Rightarrow \quad F_{h_8,8}=-F_{t7,8}-F_{t9,8}=-\frac{4\cdot T_1\cdot i_{1,3}^{h_2}\cdot i_{4,6}^{h_5}}{s_8\cdot d_7}=-24000\ \text{N}. \tag{C39}$$

- The tangential force $F_{t8,h_8}$ exerted by the center of planet gear 8 on the carrier $h_8$ (Figure C5(b)):

$$F_{t8,h_8}+F_{h_8,8}=0 \quad \Rightarrow \quad F_{t8,h_8}=-F_{h_8,8}=\frac{4\cdot T_1\cdot i_{1,3}^{h_2}\cdot i_{4,6}^{h_5}}{s_8\cdot d_7}=24000\ \text{N}. \tag{C40}$$

- The active torque $T_{h_8}$ driving the shaft of carrier $h_8$:

$$T_{h_8}=F_{t8,h_8}\cdot s_8\cdot\frac{d_7+d_8}{2}=\frac{2\cdot T_1\cdot\left(z_7+z_8\right)\cdot i_{1,3}^{h_2}\cdot i_{4,6}^{h_5}}{z_7}=2\cdot T_1\cdot\left(1-i_{7,8}^{h_8}\right)\cdot i_{1,3}^{h_2}\cdot i_{4,6}^{h_5}=11070\ \text{N}\cdot\text{m}. \tag{C41}$$

Preprints (www.preprints.org) | NOT PEER-REVIEWED | Posted: 3 August 2023 doi:10.20944/preprints202308.0223.v1



- The reaction torque $T_{h_8R}$ balancing the active torque $T_{h_8}$:

$$T_{h_8R} = F_{h_8,8} \cdot s_8 \cdot \frac{d_7 + d_9}{2} = -2 \cdot T_1 \cdot \left(1 - i_{7,8}^{h_8}\right) \cdot i_{1,3}^{h_2} \cdot i_{4,6}^{h_5} = -11070 \text{ N} \cdot \text{m} . \quad \text{(C42)}$$

## Appendix D

*D.1. Calculations of powers and power ratios of subsystem A*

- Power $P_1$ transmitted to subsystem A by the shaft I of sun gear 1 ($P_1 > 0$):

$$P_1 = T_1 \cdot \omega_1 = 1539.380 \text{ W} . \quad \text{(D1)}$$

- Power $P_3$ transmitted outside subsystem A by the shaft of ring gear 3 ($P_3 < 0$):

$$P_3 = T_{3R} \cdot \omega_3 = -P_1 \cdot \frac{i_{1,3}^{h_2}}{\left(i_{1,3}\right)_{\omega_{h2}}} = -1523.987 \text{ W} , \quad \text{(D2)}$$

where: $\left(i_{1,3}\right)_{\omega_{h2}} = \left(\frac{\omega_1}{\omega_3}\right)_{\omega_{h2}=0.154 \text{ rad/s}} = -9.09(09)$.

- Power $P_{h_2}$ transmitted outside subsystem A by the shaft of carrier $h_2$ ($P_{h_2} < 0$):

$$P_{h_2} = T_{h_2R} \cdot \omega_{h_2} = -P_1 \cdot \left(1 - \frac{i_{1,3}^{h_2}}{\left(i_{1,3}\right)_{\omega_{h2}}}\right) = -15.394 \text{ W} \quad \text{(D3)}$$

or

$$P_{h_2} = -P_1 - P_3 = -15.394 \text{ W} . \quad \text{(D4)}$$

- Power ratio in the power flow path from the input shaft I to the shaft of carrier $1_{h_2}$ (Figure 9):

$$\frac{|P_{h_2}|}{P_1} \cdot 100\% = \frac{15.394}{1539.380} \cdot 100\% = 1\% . \quad \text{(D5)}$$

- Power ratio in the power flow path from the input shaft I to the shaft of ring gear 3 (Figure 9):

$$\frac{|P_3|}{P_1} \cdot 100\% = \frac{1523.987}{1539.380} \cdot 100\% = 99\% . \quad \text{(D6)}$$

- Power ratio in the power flow paths from the input shaft I to the shafts of carrier $h_2$ and rim gear 3 (checking the absence of the power losses in subsystem A):

$$\frac{|P_{h_2}| + |P_3|}{P_1} \cdot 100\% = \frac{1539.380}{1539.380} \cdot 100\% = 100\% . \quad \text{(D7)}$$

*D.2. Calculations of powers and power ratios of subsystem B*

- Power $P_4$ transferred to subsystem B by the shaft of sun gear 4:

Preprints (www.preprints.org) | NOT PEER-REVIEWED | Posted: 3 August 2023 doi:10.20944/preprints202308.0223.v1



$$P_4 = -P_3 = T_4 \cdot \omega_4 = P_1 \cdot \frac{i_{1,3}^{h_2}}{\left(i_{1,3}\right)_{\omega_{h2}}} = 1523.987\,\text{W}\,. \qquad \text{(D8)}$$

- Power $P_{h_5}$ transmitted to subsystem B by the shaft of carrier $h_5$:

$$P_{h_5} = T_{h_5} \cdot \omega_{h_5} = -P_4 \cdot \left(1 - \frac{i_{4,6}^{h_5}}{\left(i_{4,6}\right)_{\omega_{h_5}}}\right) = -P_1 \cdot \frac{i_{1,3}^{h_2}}{\left(i_{1,3}\right)_{\omega_{h2}}} \cdot \left(1 - \frac{i_{4,6}^{h_5}}{\left(i_{4,6}\right)_{\omega_{h_5}}}\right) = 180.107\,\text{W}\,. \qquad \text{(D9}$$

where: $\left(i_{4,6}\right)_{\omega_{h5}} = \left(\frac{\omega_4}{\omega_6}\right)_{\omega_{h5}=0.154\,\text{rad/s}} = -10.732\,.$

- Power $P_6$ transmitted outside subsystem B by the shaft of ring gear 6:

$$P_6 = T_{6R} \cdot \omega_6 = -P_4 \cdot \frac{i_{4,6}^{h_5}}{\left(i_{4,6}\right)_{\omega_{h_5}}} = -P_1 \cdot \frac{i_{1,3}^{h_2}}{\left(i_{1,3}\right)_{\omega_{h2}}} \cdot \frac{i_{4,6}^{h_5}}{\left(i_{4,6}\right)_{\omega_{h_5}}} = -1704.094\,\text{W}\,. \qquad \text{(D10)}$$

or

$$P_6 = -\left(P_4 + P_{h_5}\right) = -1704.094\ \text{W}\,. \qquad \text{(D11)}$$

- Power ratio in the power flow path from the shaft of rim gear 3 to the shaft of sun gear 4 i.e. from subsystem A to subsystem B (Figure 9) :

$$\frac{P_4}{P_1} \cdot 100\% = \frac{|P_3|}{P_1} \cdot 100\% = 99\%\,. \qquad \text{(D12)}$$

- Power ratio in the power flow path from the shaft of carrier $h_5$ to subsystem B due to the coupling phenomenon (Figure 9):

$$\frac{P_{h_5}}{P_1} \cdot 100\% = 11.7\ \%\,. \qquad \text{(D13)}$$

- Power ratio in the power flow path from the shaft of rim gear 6 to the shaft of sun gear 7 i.e. from subsystem B to subsystem C (Figure 9):

$$\frac{|P_6|}{P_1} \cdot 100\% = 110.7\ \%\,. \qquad \text{(D14)}$$

- Power ratio in the power flow paths from the shafts of sun gear 4 and carrier $h_5$ to the shaft of rim gear 6 (checking for no power loss in subsystem B):

$$\frac{|P_6|}{P_4 + P_{h_5}} \cdot 100\% = 100\ \%\,. \qquad \text{(D15}$$

*D.3. Calculations of powers and power ratios of subsystem C*

- Power $P_7$ transmitted to subsystem C by the shaft of sun gear 7:

$$P_7 = -P_6 = T_7 \cdot \omega_7 = P_1 \cdot \frac{i_{1,3}^{h_2}}{\left(i_{1,3}\right)_{\omega_{h2}}} \cdot \frac{i_{4,6}^{h_5}}{\left(i_{4,6}\right)_{\omega_{h_5}}} = 1704.094\,\text{W}\,. \qquad \text{(D16)}$$

Preprints (www.preprints.org) | NOT PEER-REVIEWED | Posted: 3 August 2023 doi:10.20944/preprints202308.0223.v1



- Power $P_9$ transmitted to the fixed shaft of ring gear 9 ( $\omega_9 = 0$ ):

$$P_9 = T_{9R} \cdot \omega_9 = 0 . \qquad \text{(D17)}$$

- Power $P_{h_8}$ transmitted to the outside of the subsystem C by the shaft of carrier $h_8$ :

$$P_{h_8} = T_{h_8R} \cdot \omega_{h_8} = -P_1 \cdot \frac{i_{1,3}^{h_2}}{\left(i_{1,3}\right)_{\omega_{h2}}} \cdot \frac{i_{4,6}^{h_5}}{\left(i_{4,6}\right)_{\omega_{h_5}}} = -1704.094\,\text{W} . \qquad \text{(D18)}$$

- Power ratio in the power flow path from the shaft of rim gear 6 to the shaft of sun gear 7 i.e. from subsystem B to subsystem C (Figure 9):

$$\frac{P_7}{P_1} \cdot 100\% = \frac{1704.094}{1539.380} \cdot 100\% = 110.7\% . \qquad \text{(D19)}$$

- Power ratio in the power flow path from the shaft of sun gear 7 to the shaft of carrier $h_8$ (Figure 9):

$$\frac{\left|P_{h_8}\right|}{P_1} \cdot 100\% = \frac{1704.094}{1539.380} \cdot 100\% = 110.7\% . \qquad \text{(D20)}$$

- Power transmitted by the shaft of carrier $h_8$ from connection point with the shaft of carrier $h_5$ and before connection point with the carrier $h_2$ (Figure 4(a), Figure 5):

$$P_{h_8} + P_{h_5} = -1523.9865\,\text{W} . \qquad \text{(D21)}$$

- Power ratio in the power flow path along the shaft of carrier $h_8$ from connection point with the carriers shafts $h_5$ and before connection point with the carrier $h_2$ (Figure 9):

$$\frac{\left|P_{h_8} + P_{h_5}\right|}{P_1} \cdot 100\% = \frac{1523.986}{1539.380} \cdot 100\% = 99.0\% . \qquad \text{(D22)}$$

- Power transmitted by the output shaft II of the PGS:

$$P_{II} = P_{h_8} + P_{h_5} + P_{h_2} = -1539.380\,\text{W} . \qquad \text{(D23)}$$

- Power ratio in the power flow paths between input shaft I and output shaft II (confirmation of no power loss):

$$\frac{\left|P_{II}\right|}{P_1} \cdot 100\% = \frac{1539.380}{1539.380} \cdot 100\% = 100.0\% . \qquad \text{(D24)}$$

- The efficiency of the PGS (confirmation of no power loss):

$$\eta_{I,II} = \left| \frac{P_{h_8} + P_{h_5} + P_{h_2}}{P_1} \right| = 1 . \qquad \text{(D25)}$$

- Torque acting on the output shaft II:

$$T_{II} = -T_{IIR} = -\left(T_{h_8R} + T_{h_5} + T_{h_2R}\right) = 10000\,\text{N} \cdot \text{m} . \qquad \text{(D26)}$$

- Total gear ratio (for $\eta_{I,II} = 1$ ):

$$i_{I,II} = \frac{T_{II}}{T_I \cdot \eta_{I,II}} = \frac{10000}{10 \cdot 1} = 1000 . \qquad \text{(D27)}$$

## References


1. Davies, T. An extension of Manolescu's classification of planar kinematic chains and mechanisms of mobility M ⩾ 1, using graph theory. *Journal of Mechanisms* **1968,** 3(2), 87-100 https://doi.org/10.1016/0022-2569(68)90018-9.
2. Gogu, G. Mobility of mechanisms: a critical review. *Mech. Mach. Theory* **2005**, 40, 1068–1097 doi:10.1016/j.mechmachtheory.2004.12.014.
3. Gogu, G. Chebychev–Grübler–Kutzbach's criterion for mobility calculation of multi-loop mechanisms revisited via theory of linear transformations. *European Journal of Mechanics* **2005**, A/Solids 24, 427–441 doi:10.1016/j.euromechsol.2004.12.003.
4. Liberati, A.; Belfiore, N.P. A method for the identification of the connectivity in multi-loop kinematic chains: Analysis of chains with total and partial mobility. *Mech. Mach. Theory* **2006**, 41, 1443–1466 doi:10.1016/j.mechmachtheory.2006.01.015.
5. Huang, Z.; Liu, J.; Li, Q. A Unified Methodology for Mobility Analysis Based on Screw Theory. In Smart Devices and Machines for Advanced Manufacturing; Wang, L.; Xi. J., Eds.; Springer London, **2008**, pp. 49-76.
6. Zhua, X.; Shena,H.; Wua, C.; Chablat, D.; Yang, T. Computer-aided mobility analysis of parallel mechanisms. *Mech. Mach. Theory* **2020**, 148, 103810 https://doi.org/10.1016/j.mechmachtheory.2020.103810.
7. Laughlin, H.; Holowenko, A.; Hall, A. How to determine circulating power in controlled epicyclic gear systems. *Mach. Design* **1956,** *28* (6).
8. Gupta, A.K.; Ramanarayanan, C.P. Analysis of circulating power within hybrid electric vehicle transmissions. **Mech. Mach. Theory 2013**, Volume 64, pp. 131-143 https://doi.org/10.1016/j.mechmachtheory.2013.01.011.
9. Bottiglione, F.; De Pinto, S.; Mantriota, G. Infinitely Variable Transmissions in neutral gear: Torque ratio and power re-circulation. *Mech. Mach. Theory* **2014,** 74, 285–298 http://dx.doi.org/10.1016/j.mechmachtheory.2013.12.017.
10. H.A. Hussen, H.A.; Hussain, R.A.; Esmail, E.L.: A Simplified Algorithm for Detecting Power Recirculation within 1-Dof Multi-Entity Planetary Gear Trains. 3rd International Conference on Sustainable Engineering Techniques. IOP Conf. Series: Materials Science and Engineering **2020,** 881, 012087 IOP Publishing doi:10.1088/1757-899X/881/1/012087.
11. Chen, H.; Chen, X-A. Recirculation of Parallel-Connected Planetary Gear Trains**.** *Chinese Journal of Mechanical Engineering* **2022**, 35:27 https://doi.org/10.1186/s10033-022-00703-6.
12. Buckingham, E.H. *Spur Gears*. McGraw-Hill, New York, 1928, pp. 259-261.
13. Brandenberger, H.: Wirkungsgrad und Aufbau einfacher und zusammengesetzter Umlaufraedergetriebe. *Maschinenbau Betrieb* **1929**, 8 u. 9); pp. 249/253 u. 290/294.
14. Rudenko, N.F. *Planetary Gears, 3rd ed.,* Mashgiz **1947**, 3rd Edition (in Russian).
15. Surowiak, W. *Planetary gears*. PWT Warsaw **1959** (in Polish).
16. Müller, H.W. *Die Umlaufgetriebe*. Springer-Verlag. Berlin Heidelberg **1971** (in Germany).
17. J. Volmer, J.; F. Leistner, F.; Wilhelm, O. *Getriebetechnik Umlaufrädergetriebe*, VEB Verlag Technik **1972** (in Germany).
18. Kudrjavtzev, V.N.; Kirdjashev, Ju.N. Eds. *Planetary Gears – Handbook*. Mashinostroenie Moskwa **1977** (in Russian).
19. Müller, L. *Planetary gears*. PWN Warsaw **1983** (in Polish).
20. Looman, J. *Zahnradgetriebe*. Springer-Verlag Berlin, Heidelberg **1996** (in Germany).
21. Müller, L.; Wilk A. *Planetary Gears*. PWN Warsaw **1996** (in Polish).
22. Tsai , L. W.; *Mechanism Design: Enumeration of Kinematic Structure According to Function* ,CRC, Boca Raton, FL 2001
23. Arnaudov, K., Karaivanov, D.P. *Planetary Gear Trains*. CRC Press. Taylor&Francis Group. London, New York 2019.
24. Krukowski, A. *Fundamentals of planetary gear theory*. In Machine Design Basics. Dietrich, M. Ed., PWN **1991**, Volume IV, pp. 330-360 (in Polish).
25. Radzimovsky, E.I. A Simplified Approach for Determining Power Losses and Efficiency of Planetary Gear Drives. *Mach. Design* **1956**, 28, pp. 101–110.
26. Radzimovsky, E.I. How to find efficiency, speed and power losses in planetary gear drives. *Mach. Design* **1959**, 31, 144–153.

27. Macmillan, R.H. Power flow and loss in differential mechanisms. *J. Mech. Eng. Sci*. 3 (**1961**) 37–41.
28. Sanger, D. The determination of power flow in multiple-path transmission systems. *Mech. Mach. Theory* **1972**, 7, pp. 103–109.
29. Salgado, D.R.; Del Castillo, J.M. Selection and Design of Planetary Gear Trains Based on Power Flow Maps. *J. Mech. Des*. **2005**, 127(1): 120-134 (15 pages) https://doi.org/10.1115/1.1828458.
30. Bu, Z., Liu, G., Wu, L., Liu, Z. Kinematics and Statics Analysis for Power Flow Planet Gear Trains. In *Global Design to Gain a Competitive Edge.* Yan, X-T., Eynard. B., Ion, W., J., Eds.; Publisher: Springer-Verlag London Limited, 2008; pp. 631–640.
31. Dooner, D., Yoon, H-D., Seireg, A. Kinematic considerations for reducing the circulating power effects in gear-type continuously variable transmissions. *Proc IMechE, Part D: J. Automobile Engineering*, **1998**, 212 (6) https://doi.org/10.1243/0954407981526118.
32. Hedman A. Transmission Analysis—Automatic Derivation of Relationships. *J. Mech. Des.* **1993**, *115(4): 1031-1037 (7 pages)* https://doi.org/10.1115/1.2919252.
33. Rabindran, D., Tesar, D. ParametricDesign and Power-Flow Analysis of Parallel Force/Velocity Actuators. *J. of Mechanisms and Robotics* **2009**, 1, 011007-1.
34. Rabindran, D., Tesar, D. ParametricDesign of Parallel Force/Velocity Actuators: Force Distribution Analysis. *J. of Mechanisms and Robotics* **2010**, 2, 011013-1.
35. Wang, C., Cui H-y. The analysis of power circulation and the simplified expression of the transmission efficiency of 2K-H closed epicyclic gear trains. Meccanica **2013**, 48:1071–1080 DOI 10.1007/s11012-012-9652-0.
36. Arnaudov, K.; Karaivanov, D. Alternative Method for Analysis of Complex Compound Planetary Gear Trains: Essence and Possibilities. G. Dobre (ed.), Power Transmissions, Mechanisms and Machine Science 13, Springer Science+Business Media Dordrecht 2013 DOI: 10.1007/978-94-007-6558-0_1.
37. Jianying, L., Qingchun, H. Power analysis and efficiency calculation of the complex and closed planetary gears transmission. *Energy Procedia* **2016**, 100, 423-433.
38. Nutakor, C.; Kłodowski, A.; Sopanen, J.; Mikkola, A.; Pedrero, J.I. Planetary gear sets power loss modeling: application to wind turbines. *Tribol. Int*. **2017**, 105:42–54 https://doi.org/10.1016/j.triboint.2016.09.029.
39. Theochari, G.; Troha, S.; Karaivanov, D. Reducer with a planetary gear train for a hoisting mechanism of dangerous goods cranes. Int. Scient. *J. "Trans & Motauto World"* **2020**. Web Issn 2534-8493; Print ISSN 2367-8399.
40. Hussen, H.A.;Essam Lauibi Esmail, E.L.; Hussen, R.A. Power Flow Simulation for Two-Degree-of-Freedom Planetary Gear Transmissions with Experimental Validation. *Hindawi Modelling and Simulation in Engineering* **2020**, Article ID 8837605, 14 pages https://doi.org/10.1155/2020/8837605.
41. Sun, Z., Gao, B., Jin, J., Sanada, K. Power Loss Evaluation of Automated Manual Transmission with Gearshift Assistant Mechanism. *International J. of Automotive Technology*, **2021**, 22(2), pp. 441–454 (2021) DOI 10.1007/s12239–021–0041–3.
42. Kahraman, A.; Ligata, H.; Kienzle, K.; Zini, D.M. A Kinematics and Power Flow Analysis Methodology for Automatic Transmission Planetary Gear Trains. J. *Mech. Des*. **2004**, 126(6): 1071-1081 (11 pages) https://doi.org/10.1115/1.1814388.
43. Dong, P.; Liu, Y.; Tenberge, P.; Xu, X. Design and analysis of a novel multi-speed automatic transmission with four degrees-of-freedom. *Mech. Mach. Theory* **2017**, 108, pp. 83–96 https://doi.org/10.1016/j.mechmachtheory.2016.10.013.
44. Liu, J.; Yu, L.; Zeng, Q.; Li, Q. Synthesis of multi-row and multi-speed planetary gear mechanism for automatic transmission. *Mech. Mach. Theory* **2018**, 128, pp. 616–627 https://doi.org/10.1016/j.mechmachtheory.2018.07.007.
45. Hwang, W.-M.; Huang, Y.-L. Connecting clutch elements to planetary gear trains for automotive automatic transmissions via coded sketches. *Mech. Mach. Theory* **2011**, 46, pp. 44–52 doi:10.1016/j.mechmachtheory.2010.08.013.
46. Ciobotaru, T.; Frunzeti, D.; Rus, I.; Jantschi, L. Method for analyzing multi-path power flow transmissions, *Proc IMechE, Part B: J Engineering Manufacture* **2009**, 224 (9), 1447–1454 https://doi.org/10.1243/09544054JEM1668.
47. Chen, H.; Chen, X. A. New Methodology for Multistage Multispeed Planetary Transmission Design Based on Geometry. *J. Mech. Des*. **2021**, 143(11): 113401 https://doi.org/10.1115/1.4050745.

48. Hedman, A. Transmission Analysis-Automatic Derivation of Relationships. *J. Mech. Des*. **1993**, 115(4), 1031-1037 https://doi.org/10.1115/1.2919252.
49. Zhang, Q.; Liu, X. Optimization of the Quality of the Automatic Transmission Shift and the Power transmission Characteristics. *Energies* **2022**, 15, 4672. https://doi.org/10.3390/en15134672.
50. Zhang, W.; Yang, J.; Zhang, W. Influence of a New Type of Two-Speed Planetary Gear Automatic Transmission on the Performance of Battery Electric Vehicles. *Energies* **2022**, 15, 4162 https://doi.org/10.3390/en15114162.
51. Mangialardi, L.; Mantriota, G. The advantages of using continuously variable transmission in wind power systems. *Renewable Energy*, **1992**, 2(3), pp. 201–209.
52. L. Mangialardi, G. Mantriota, Power flows and efficiency in infinitely variable transmissions, *Mech. Mach. Theory* **1999**, Volume 34. Pp. 973–994.
53. Mantriota, G., Theoretical and experimental study of power split CVT systems: part I, *Proc IMechE, Part D: J Automobile Engineering*. **2001,** 215 (D7), pp. 837–850 https://doi.org/10.1243/0954407011528428.
54. Mantriota, G. Theoretical and experimental study of power split CVT systems: part II, *Proc IMechE, Part D: J Automobile Engineering* **2001**, 215 (D7), pp. 851–864 https://doi.org/10.1243/0954407011528428.
55. Mucino, V.H.; Lu, Z.; Smith, J.E.; Kimcikiewicz, M.; Cowan, B. Design of continuously variable power split transmission systems for automotive applications, *Proc IMechE, Part D: J Automobile Engineering* **2001**, 215, 469–478, https://doi.org/10.1243/0954407011528086.
56. Mantriota, G. Performances of a series infinitely variable transmission with type I power flow, *Mech. Mach. Theory* **2002**, 37 (6), pp. 579–597 https://doi.org/10.1016/S0094-114X(02)00017-4.
57. Mantriota, G. Performances of a parallel infinitely variable transmissions with a type II power flow, *Mech. Mach. Theory* **2002**, 37 (6), pp. 555–578 https://doi.org/10.1016/S0094-114X(02)00018-6.
58. Zhao, X.; Maißer. P. A novel power splitting drive train for variable speed wind power generators. *Renewable Energy* **2003**, 28, pp. 2001–2011 doi:10.1016/S0960-1481(03)00127-7.
59. Linares, P.; Méndez, V.; Catalán, H. Design parameters for continuously variable power-split transmissions using planetaries with 3 active shafts. *J. Terramechanics* **2010**, 47, pp. 323–335 doi:10.1016/j.jterra.2010.04.004.
60. Macor, A.; Rossett. A. Optimization of hydro-mechanical power split transmissions. *Mech. Mach. Theory* **2011**, 46, 1901–1919 doi:10.1016/j.mechmachtheory.2011.07.007.
61. Bottiglione, F.; Mantriota, G. Power Flows and Efficiency of Output Compound e-CVT. Intern. *J. Vehicle Design*, **2015**, Article ID 136437, 12 pages http://dx.doi.org/10.1155/2015/136437.
62. Mantriota, G. Power split transmissions for wind energy systems. *Mech. Mach. Theory* **2017**, 117, 160–174 http://dx.doi.org/10.1016/j.mechmachtheory.2017.07.003.
63. Esmail, E.L. Comments on "Power flow and efficiency analysis of epicyclic gear transmission with split power", *Mech. Mach. Theory* **2017**, 115, pp. 237–243.
64. Esmail, E.L. Comments on "Analysis of circulating power within hybrid electric vehicle transmissions", *Mech. Mach. Theory* **2013**, 64, pp. 131–143, by A.K. Gupta, C.P. Ramanarayanan https://doi.org/10.1016/j.mechmachtheory.2017.11.001.
65. Cammalleri, M.; Rotella, D. Functional design of power-split CVTs: An uncoupled hierarchical optimized model. *Mech. Mach. Theory* **2017**, 116, pp. 294–309 http://dx.doi.org/10.1016/j.mechmachtheory.2017.06.003.
66. Rotella, D., Cammalleri, M. Direct analysis of power-split CVTs: A unified method. *Mech. Mach. Theory* **2018**, 121, pp. 116-127
67. Rotella, D., Cammalleri, M. Power losses in power-split CVTs: A fast black-box approximate method. *Mech. Mach. Theory* **2018**, 128, pp. 528–543 https://doi.org/10.1016/j.mechmachtheory.2018.06.011.
68. Xiong, S.; Wilfong, G.; Lumkes Jr., J. Components Sizing and Performance Analysis of Hydro-Mechanical Power Split Transmission Applied to a Wheel Loader. *Energies* **2019**, 12, 1613; doi:10.3390/en12091613.
69. Wang, G.; Song, Y.; , Wang, J.; Wanqiang Chen, W.; Cao, Y.; Wang, J. Study on the Shifting Quality of the CVT Tractor under Hydraulic System Failure. *Appl. Sci*. **2020**, 10, 681; doi:10.3390/app10020681.
70. Neagoe, M.; Saulescu, R.; Jaliu, C.; Simionescu, P.A. A Generalized Approach to the Steady-State Efficiency Analysis of Torque-Adding Transmissions Used in Renewable Energy Systems. *Energies* **2020**, 13, 4568; doi:10.3390/en13174568.
71. Lin, A.-D.; Hung, T.-D.; Kuang, J.-H.; Tsai, H.-A. Power Flow Analysis on the Dual Input Transmission Mechanism of Small Wind Turbine Systems. *Appl. Sci*. 2020, 10, 7333; doi:10.3390/app10207333.
72. Mantriota, G.; Reina, G.; Ugenti, A. Performance Evaluation of a Compound Power-Split CVT for Hybrid Powertrains. *Appl. Sci*. **2021**, 11, 8749. https://doi.org/10.3390/app11188749.

73. Li, Q.; Zhang, Z.; Bai, J.; Zhang, T.; Gai, F. Development of compound power-split hybrid power system for commercial vehicles. *Int. Journal of Automotive Technology*, **2022**, 23(1), pp. 135-147 DOI 10.1007/s12239-022-0011-4.
74. Li, X.; Kang, X.; Ba. X.; Peng, Z.; Yang, S.; Zhao, Z. A Design Methodology for Dual-Mode Electro-Mechanical Transmission Scheme Based on Jointing Characteristics. *Energies* **2022**, 15, 5482 https://doi.org/10.3390/en15155482.
75. Kukla, M.; Wieczorek, B.; Warguła, Ł.; Rybarczyk, D.; Górecki, J. Manual Wheelchair Equipped with a Planetary Gear-Research Methodology and Preliminary Results. *Appl. Sci.* **2022**, 12, 7737. https://doi.org/10.3390/app12157737.
76. Wang, L.; Cui, Y.; Zhang, F.; Li, G. Architectures of Planetary Hybrid Powertrain System: Review, Classification and Comparison. *Energies* **2020**, 13, 329; doi:10.3390/en13020329.
77. Ngo, H.-T.; Yan, H.-S. Configuration synthesis of parallel hybrid transmissions. *Mech. Mach. Theory* **2016**, 97, pp. 51–71 http://dx.doi.org/10.1016/j.mechmachtheory.2015.11.002.
78. Yang, F; Feng, J.; Du F. Design and Power Flow Analysis for Multi-Speed Automatic Transmission with Hybrid Gear Trains. *Int. J. of Automotive Technology*, **2016**, 17, 4, pp. 629−637 DOI 10.1007/s12239−016−0062−5.
79. Ahn, K.; Cho, S.-t.; Lim, W.; Park, Y-I.; Lee, J.M. Performance analysis and parametric design of the dual-mode planetary gear hybrid powertrain. *Proc IMechE Part D: J. Automobile Engineering* **2006**, 220(11), https://doi.org/ 10.1243/09544070JAUTO334.
80. Kim, N.; Kim, J.; Kim, H. Control of Dual Mode Power Split Transmission for a Hybrid Electric Vehicle. *World Electric Veh. J.* **2008**, 2(4), ISSN 2032-6653.
81. Cammalleri, M.; Castellano, A. Analysis of hybrid vehicle transmissions with any number of modes and planetary gearing: kinematics, power flows, mechanical power losses. *Mech. Mach. Theory* **2021**, 162, 104350 https://doi.org/10.1016/j.mechmachtheory.2021.104350.
82. Li, Q.; Zhang, Z.; Zhang, T.; Guo, H. Control optimization of a compound power-split hybrid power system for commercial vehicles. *Proc IMechE Part D: J. Automobile Engineering* **2021**, 235(9) https://doi.org/10.1177/0954407021993639.
83. van Harselaar, W.; Brouwer, M.; Hofman, T. A generic transmission model for hybrid electric drives. *Forsch Ingenieurwes*. **2019** 83:1–9 https://doi.org/10.1007/s10010-018-00295-5 F.
84. Yang, F.; Feng, J.; Zhang, H. Power flow and efficiency analysis of multi-flow planetary gear trains. *Mech. Mach. Theory* **2015**, 92, 86–99 http://dx.doi.org/10.1016/j.mechmachtheory.2015.05.003.
85. Yin, C.; Tang, D.; Deng, Z. Research on configurations of multi-axis speed-differential mechanisms based on 2K-H gear train. *Mech. Mach. Theory* **2020**, 148, 103783 https://doi.org/10.1016/j.mechmachtheory.2020.103783.
86. Gu, J.; Zhao, Z.; Chen, Y.; He, L.; Zhan, X.. Integrated optimal design of configuration and parameter of multimode hybrid powertrain system with two planetary gears. *Mech. Mach. Theory* **2020**, 143, 103630 https://doi.org/10.1016/j.mechmachtheory.2019.103630.
87. Kim, H.; Wi, J.; Yoo, J.; Son, H.; Park, C.; Kim, H. A Study on the Fuel Economy Potential of Parallel and Power Split Type Hybrid Electric Vehicles. *Energies* **2018**, 11, 2103; doi:10.3390/en11082103.
88. De Carlo, M.; Mantriota, G. Electric vehicles with two motors combined via planetary gear train. *Mech. Mach. Theory* **2020**, 148, 103789 https://doi.org/10.1016/j.mechmachtheory.2020.103789.
89. Mantriota, G. and Reina, G. Dual-Motor Planetary Transmission to Improve Efficiency in Electric Vehicles. *Machines* **2021**, 9, 58. https://doi.org/10.3390/machines9030058.
90. Cipek, M.; Pavkovic′, D.; Petric J. A control-oriented simulation model of a power-split hybrid electric vehicle. *Applied Energy* **2013**, 101, pp. 121–133 http://dx.doi.org/10.1016/j.apenergy.2012.07.006.
91. Son, H.; Kim, H. Development of Near Optimal Rule-Based Control for Plug-In Hybrid Electric Vehicles Taking into Account Drivetrain Component Losses. *Energies* **2016**, 9, 420; doi:10.3390/en9060420.
92. Yang, W.; Liang, J.; Yang, J.; Zhang, N. Investigation of a Novel Coaxial Power-Split Hybrid Powertrain for Mining Trucks. *Energies* **2018**, 11, 172; doi:10.3390/en1101017.
93. Kim, S.J; Kim, K.-S. Experimental Investigation of the Seamless Gearshift Mechanism Using an Electric Motor and a Planetary Gear-Set. *Energies* **2020**, 13, 6705; doi:10.3390/en13246705.
94. Kim, J.; Kang, J.; Kim, Y.; Kim, T.; Min, B.; Kim, H. Design Of Power Split Transmission: Design Of Dual Mode Power Split Transmission. *Int. J. Automotive Technology*, **2010**, 11 (4), pp. 565−571 DOI 10.1007/s12239−010−0068−3. Lever kinem-statyka

95. Wang, W.; Song, S.; Guo, M.; Liu, S. Analysis on compound-split configuration of power-split hybrid electric vehicle. *Mech. Mach. Theory* **2014**, 78, pp. 272–288 http://dx.doi.org/10.1016/j.mechmachtheory.2014.03.019.
96. Esmail, E.L. Hybrid Transmission for Mobile Robot. *J. Mech. Des*. **2012**, 134(2): 021001 https://doi.org/10.1115/1.4005590
97. Ho, T.-T.; H, S.-J. Configuration synthesis of two-mode hybrid transmission systems with nine-link mechanisms. *Mech. Mach. Theory* **2019,** 142, 103615.
98. Ngo, H.-T., Yan, H.-S. Configuration synthesis of parallel hybrid transmissions. *Mech. Mach. Theory* **2016**, 97, 51–71 http://dx.doi.org/10.1016/j.mechmachtheory.2015.11.002.
99. Li, H.; Hu, X.; Fu, B.; Wang, J.; Zhang, F.; Zhou, Y. Effective optimal control strategy for hybrid electric vehicle with continuously variable transmission. *Adv. Mech. Eng*. **2019**, Vol. 11(3) 1–11 DOI: 10.1177/1687814018824811.
100. Yang, H.; Chom S.; Kim, N.; Lim, W.; Cha, S. Analysis of Planetary Gear Hybrid Powertrain System. Part 1: Input Split System. *Intern. J. Automotive Techn*. **2007**, 8 (6), pp. 771−780 DOI 10.1007/s12239−009−0044−y.
101. Yang, H.; Kim, N.; Par, Y.; Lim, W.; Cha, S. Analysis of Planetary Gear Hybrid Powertrain System. Part 2: Output Split System. *Intern. J. Automotive Techn*. **2009**, 10 (3), pp. 381−390 DOI 10.1007/s12239−009−0044−y.
102. Schulz, M. Circulating mechanical power in a power-split hybrid electric vehicle transmission. *Proc IMech Part D: J. Automobile Engineering* **2004**, 218(12), 1419−1425 https://doi.org/10.1243/0954407042707759.
103. Kim, I.; Kim, H. Configuration Analysis of Plug-in Hybrid Systems using Global Optimization. *World Electric Vehicle Journal* **2013**, 6 - ISSN 2032-6653.
104. Szumanowski, A.; Liu, Z.; Krawczyk, P. Analyse of Clutch-brake System Control Based on Experimental Tests and Applied in Hybrid Power Train. *World Electric Vehicle Journal* **2013**, 6 - ISSN 2032-6653.
105. Zou, Y.; Huang, R.; Wu, X.; Zhang, B.; Zhang, Q.; Wang, N.; Qin, T. Modeling and energy management strategy research of a power-split hybrid electric vehicle. *Adv. Mech. Eng*. **2020**, 12 (10), pp. 1–14 DOI: 10.1177/1687814020962624.
106. De Pinto, S.; Mantriota, G. Power Flows in Compound Transmissions for Hybrid Vehicles. *Machines* **2019**, 7, 19; doi:10.3390/machines7010019.
107. Gu, J.; Zhao, Z.; Chen, Y.; He, L.; Zhan, X. Integrated optimal design of configuration and parameter of multimode hybrid powertrain system with two planetary gears. *Mech. Mach. Theory* **2020**, 143, 103630 https://doi.org/10.1016/j.mechmachtheory.2019.103630.
108. Mazali, I.I., Zul Hilmi Che Daud, Z.H., Hamid, M.K. et al. Review of the Methods to Optimize Power Flow in Electric Vehicle Powertrains for Efficiency and Driving Performance. *Appl. Sci*. **2022**, 12, 1735. https://doi.org/10.3390/app12031735.
109. Wang, S.; Li, J.; Shi, D.; Sun, X.; Yao, Y. Energy Management Strategy of Dual Planetary Hybrid Electric Vehicle Based on Optimal Transmission Efficiency. *J. Theor. Appl. Mech*. **2019**, 57, (2), pp. 383-396, DOI: 10.15632/jtam-pl/104591.
110. Huang, K.; Xiang, C.; Ma, Y.; Wang, W.; Langari, R. Mode Shift Control for a Hybrid Heavy-Duty Vehicle with Power-Split Transmission. *Energies* **2017**, 10, 177; doi:10.3390/en10020177.
111. Li, L.;Yana,B.; Songa, J.; Zhanga, Y.; Jiang, G.; Li, L. Two-step optimal energy management strategy for single-shaft series-parallel powertrain. *Mechatronics* **2016**, 36, 147–158.
112. Zhang, D.; Chen, J.; Hsieh, J.; Rancourt, J.; Schmidt, M.R. Dynamic modelling and simulation of two-mode electric variable transmission. *Proc IMechE, Part D: J Automobile Engineering* **2001**, 215(11) https://doi.org/10.1243/0954407011528743.
113. Wang, W.; Song, R.; Guo, M, Liu. S. *Mech. Mach. Theory* **2014**, Analysis on compound-split configuration of power-split hybrid electric vehicle. *Mech. Mach. Theory* **2014**, 78, 272–288 doi.org/10.1016/j.mechmachtheory.2014.03.019 0094-114X.
114. Yaohua, L.; Wang Ying, W.; Xuan, Z. Modelling and Simulation Study on a Series-parallel Hybrid Electric Vehicle. *World Electric Vehicle Journal* **2015**, 7 - ISSN 2032-6653.
115. Chen, H.; Li, L.; Küçükay, F. Study of Series-Parallel and Power-Split DHT for Hybrid Powertrains. *Automotive Innovation* **2021,** 4:23–33 https://doi.org/10.1007/s42154-020-00126-w.
116. Son, H.; Kim, H. Development of Near Optimal Rule-Based Control for Plug-In Hybrid Electric Vehicles Taking into Account Drivetrain Component Losses. *Energies* **2016**, 9, 420; doi:10.3390/en9060420.

117. Weichao Zhuang, W.; Zhang, X.; Peng, H.; Wang, L. Simultaneous Optimization of Topology and Component Sizes for Double Planetary Gear Hybrid Powertrains. *Energies* **2016**, 9, 411; doi:10.3390/en9060411.
118. Wu, J.; Liang, J.; Ruan, J.; Zhang, N.; Walker, P.D. Efficiency comparison of electric vehicles powertrains with dual motor and single motor input. *Mech. Mach. Theory* **2018**, 128, pp. 569–585 https://doi.org/10.1016/j.mechmachtheory.2018.07.003.
119. Liang, J.; Yang, H.; Wu, J.; Zhang, N.; Walker, P.D. Shifting and power sharing control of a novel dual input clutchless transmission for electric vehicles. *Mechanical Systems and Signal Processing* **2018**, 104, pp. 725–743 https://doi.org/10.1016/j.ymssp.2017.11.033.
120. Tom Verstraten, T.; Furnémont, R.; López-García, P.; Rodriguez-Cianca, D.; Cao, H.-L.; Vanderborght, B.; Lefeber, D. Modeling and design of an energy-efficient dual-motor actuation unit with a planetary differential and holding brakes. *Mechatronics* **2018**, 49, pp. 134-148 https://doi.org/10.1016/j.mechatronics.2017.12.005.
121. Han, J.-O.; Shin, J.-W.; Kim, J.-C.; Oh, S.-H. Design 2-Speed Transmission for Compact Electric Vehicle Using Dual Brake System. *Appl. Sci*. **2019**, 9, 1793; doi:10.3390/app9091793.
122. Hu, J.; Mei, B.; Peng, H.; Jiang, X. Optimization Design and Analysis for a Single Motor Hybrid Powertrain Configuration with Dual Planetary Gears. *Appl. Sci*. **2019**, 9, 707; doi:10.3390/app9040707.
123. Zhao, X.; Tang, J. Modeling and Optimal Shift Control of a Planetary Two-Speed Transmission. *World Electric Vehicle Journal* **2019**, 10, 53; doi:10.3390/wevj10030053.
124. Nazari, S.; Siegel, J.; Middleton, R.; Stefanopoulou, A. Power Split Supercharging: A Mild Hybrid Approach to Boost Fuel Economy. *Energies* **2020**, 13, 6580; doi:10.3390/en13246580.
125. Tota, A.; Galvagno , E.; Dimauro, L.; Vigliani, A.; Velardocchia, M. Energy Management Strategy for Hybrid Multimode Powertrains: Influence of Inertial Properties and Road Inclination. *Appl. Sci*. **2021**, 11, 11752. https://doi.org/10.3390/app112411752.
126. Castellano, A.; Cammalleri, M. Power Losses Minimization for Optimal Operating Maps in Power-Split HEVs: A Case Study on the Chevrolet Volt. *Appl. Sci*. **2021**, 11, 7779. https://doi.org/10.3390/app11177779.
127. Yang, W.; Li, C. Symmetry Detection and Topological Synthesis of Mechanisms of Powertrains. *Energies* **2022**, 15, 4755 https://doi.org/10.3390/en15134755.
128. Chen, X.; Jiang, J.; Zheng, L.; Tang, H.; Chen, X. Study and Analysis of a Multi-Mode Power Split Hybrid Transmission. *World Electric Vehicle Journal* **2020**, 11, 46; doi:10.3390/wevj11020046.
129. Yang, F.; Feng, J.; Zhang H. Power flow and efficiency analysis of multi-flow planetary gear trains. *Mech. Mach. Theory* **2015**, Volume 92, pp. 86-99 https://doi.org/10.1016/j.mechmachtheory.2015.05.003.
130. Dong, P.; Zuo, S.; Liu, T.; Xu, X.; Guo, W.; Liu, Y.; Wu, H.; Wang, S. A matrix-based method for searching configurations of planetary gear trains. *Mech. Mach. Theory* **2023**, 180, 105161 https://doi.org/10.1016/j.mechmachtheory.2022.105161.
131. Benford, H.L.; Leising, M.B. The Lever Analogy: A New Tool in Transmission Analysis. *SAE Trans*. **1981**, 90, 429–437. DOI: https://doi.org/10.4271/810102.
132. Esmail, E.L.; Hussen, H. Nomographs for Kinematics, Statics and Power Flow Analysis of Epicyclic Gear Trains. Conference Paper **2009** ASME International Mechanical Engineering Congress and Exposition.
133. Esmail, E.L.; Pennestrì, E.; Juber, A.H. Power Losses in Two-Degrees-of-Freedom Planetary Gear Trains: A Critical Analysis of Radzimovsky's Formulas. *Mech. Mach. Theory* **2018**, 128, pp. 191–204 https://doi.org/10.1016/j.mechmachtheory.2018.05.015.
134. Marciniec, A.; Sobolak, M.; Połowniak, P. Graphical method for the analysis of planetary gear trains. *Alexandria Engineering Journal* **2022**, *61, 5,* pp. 4067-4079 https://doi.org/10.1016/j.aej.2021.09.036.
135. Xie, T.; Hu, J.; Peng, Z.; Liu, C. Synthesis of seven-speed planetary gear trains for heavy-duty commercial vehicle. *Mech. Mach. Theory* **2015**, 90, pp. 230–239 http://dx.doi.org/10.1016/j.mechmachtheory.2014.12.012.
136. Zhang, Y.; Ma, X.; Yin, C.; Yuan, S. Development and Simulation of a Type of Four-Shaft ECVT for a Hybrid Electric Vehicle. *Energies* **2016**, 9, 141; doi:10.3390/en9030141.
137. Liao, Y.G.; Chen, M.-Y. Analysis of multi-speed transmission and electrically continuous variable transmission using lever analogy method for speed ratio determination. *Adv. Mech. Eng*. **2017**, 9(8), 1–12 DOI: 10.1177/1687814017712948.
138. Ho, T.-T.; Hwang, S.-J. Configuration Synthesis of Novel Hybrid Transmission Systems Using a Combination of a Ravigneaux Gear Train and a Simple Planetary Gear Train. *Energies* **2020**, 13, 2333 doi:10.3390/en13092333.

139. Yang, X.; Yu, W.; Shao, Y.; Xu. Z.; Zeng, Q.; Nie, C.; Peng, D. An Augmented Lever Analogy Method for Kinematic Analysis of Dual-Input Planetary/Epicyclic Gear Sets Involving Planet Gear. IEEE*Access* **2022**, 10.1109/ACCESS.2022.3206845.
140. Chen, X-A.; Chen, H. Analytical geometry method of planetary gear trains. *SCIENCE CHINE Technological Sciences* **2012**, 55 (4), pp. 1007-1021 doi: 10.1007/s11431-011-4736-y.
141. Del Castillo, J.M. The Analytical Expression of the Efficiency of Planetary Gear Trains. *Mech. Mach. Theory* **2002**, 37, pp. 197-214. https://doi.org/10.1016/S0094-114X(01)00077-5.
142. Chen, C.; Angeles, J. Virtual-power flow and mechanical gear-mesh power losses of epicyclic gear trains. *J. Mech. Des*. **2007**, 129(1), pp. 107–113 https://doi.org/10.1115/1.2359473.
143. Chen, C.; Liang, T.T. Theoretic Study of Efficiency of Two-DOFs of Epicyclic Gear Transmission via Virtual Power. J. Mech. Design **2011**, 133(3), 031007 DOI 10.1115/1.4003568.
144. Chen, C. Power Analysis of Epicyclic Transmissions Based on Constraints. *J. Mechanisms Robotics* **2012**, 4(4), 041004 (11 pages) https://doi.org/10.1115/1.4007308. Lagrange multipliers and newly introduced selection matrices.
145. Chen, C. Power Flow and Efficiency Analysis of epicyclic gear transmission with split power. *Mech. Mach. Theory* **2013**, 59, pp. 96-106 http://dx.doi.org/10.1016/j.mechmachtheory.2012.09.004.
146. Chen, C.; Chen, J. Power analysis of two-dof epicyclic gear transmission and experimental validation, in: International Gear Conference, Lyon, **2014**, pp. 646–658
147. Chen, C.; Chen, J. Efficiency analysis of two degrees of freedom epicyclic gear transmission and experimental validation. *Mech. Mach. Theory* **2015**, 87, pp. 115-130 http://dx.doi.org/10.1016/j.mechmachtheory.2014.12.017.
148. Wang, C. The effect of planetary gear/star gear on the transmission efficiency of closed differential double helical gear train. *Proc IMech, Part C: J. Mechanical Engineering Science* **2019**, 233 5647-5658 https://doi.org/10.1177/0954406220921205.
149. Chen, C. Power Flow analysis of Compound Epicyclic Gear Transmission: Simpson Gear Train. *J. Mech. Design* **2011**, 133(9), 094502 DOI: 10.1115/1.4004609.
150. Li, J.; Wu, T.; Chi, W.; Hu, Q.; Meen, T. Integrated Analysis of Influence of Multiple Factors on Transmission Efficiency of Loader Drive Axle. *Energies* **2019**, 12, 4540 doi:10.3390/en12234540.
151. Esmail, E.L.; Pennestri, E.; Cirelli, M. Power-Flow and Mechanical Efficiency Computation in Two-Degrees-of-Freedom Planetary Gear Units: New Compact Formulas. *Appl. Sci*. **2021**, 11, 5991. https://doi.org/10.3390/app11135991.
152. Wojnarowski J. Letters to the Editor Comments on "The Determination of Power Flow in Multiple-Path Transmission Systems" In Sanger, D. *Mech. Mach. Theory* **1972**, 7 (1), pp. 103-109]. *Mech. Mach. Theory*. **1975**. 10, pp. 261-266.
153. Wojnarowski, J.; Lidwin A. The application of signal flow graphs—the kinematic analysis of planetary gear trains. *Mech. Mach. Theory* **1975**, 10(1), pp.17-31 https://doi.org/10.1016/0094-114X(75)90054-3.
154. Wojnarowski, J. The Graph Method of Determining the Loads in Complex Gear Trains. *Mech. Mach. Theory* **1976**, 11(2), pp.103–121 https://doi.org/10.1016/0094-114X(76)90003-3.
155. Pennestri, E.; Freudenstein, F. A systematic approach to power-flow and static-force analysis in epicyclic spur-gear trains. *J. Mech. Des*. **1993**, 115(3), pp. 639-644 https://doi.org/10.1115/1.2919238.
156. Pennestri, E.; Freudenstein, F. The Mechanical Efficiency of Epicyclic Gear Trains. *J. Mech. Design* **1993**, 115(3), pp. 645-651 https://doi.org/10.1115/1.2919239.
157. Valentini, P.P.; Pennestri, E.; A Review of Formulas for the Mechanical Efficiency Analysis of Two Degrees-of-Freedom Epicyclic Gear Trains. *J. Mech. Design* **2003**, 125(3), pp. 602-608 https://doi.org/10.1115/1.1587157.
158. Pennestri, E.; Mariti, L.; Valentini, P.P.; Mucino, V.H. Efficiency evaluation of gearboxes for parallel hybrid vehicles: Theory and applications. *Mech. Mach. Theory* **2012**, 49, pp. 157-176 doi:10.1016/j.mechmachtheory.2011.10.012.
159. Del Pio, G.; Pennestri E.; Valentini, P.P. Kinematic and power-flow analysis of bevel gears planetary gear trains with gyroscopic complexity. *Mech. Mach. Theory* **2013**, 70, pp. 523-537 http://dx.doi.org/10.1016/j.mechmachtheory.2013.08.016.
160. Geitner, G,-H.; Kömürgöz, G. Generic power split modelling for compound epicyclic four speed gears. *Mech. Mach. Theory* **2017**, 116C, 50-68.

161. Geitner, G,-H.; Kömürgöz, G. Bond Graph Based Synthesis of Generic Power Split Modelling for Epicyclic Four-Speed Gears. In Graph-Based Modelling in Science, Technology and Art, Zawiślak, S.; Rysiński J. Eds. Springer 2022
162. Li, J.; Hu, Q. Power analysis and efficiency calculation of the complex and closed planetary gears transmission. *Energy Procedia* **2016**, 100, pp. 423-433.
163. Salgado, D.R.; del Castillo, J.M. Analysis of the transmission ratio and efficiency ranges of the four-, five-, and six-link planetary gear trains. *Mech. Mach. Theory* **2014**, 73, pp. 218–243 https://doi.org/10.1016/j.mechmachtheory.2013.11.001.
164. Pennestrì, E.; Belfiore, N.P. On Crossley's contribution to the development of graph based algorithms for the analysis of mechanisms and gear trains. *Mech. Mach. Theory* **2015**, 89, 92–106 http://dx.doi.org/10.1016/j.mechmachtheory.2014.09.001.
165. Cui, Y.; Gao, J.; Ji, X.; Zhou, X.; Yan, H. The multi-attribute topological graph method and its application on power flow analysis in closed planetary gear trains. *J. Adv. Mech. Eng*. **2018**, 10 (8), https://doi.org/10.1177/1687814018794103.
166. Esmail, E.L.; Hassan, S.S. An approach to power-flow and static force analysis in multi-input multi-output epicyclic-type transmission trains. *J. Mech. Design* **2010**, 132 (1): 0110091–01100910 https://doi.org/10.1115/1.4000644.
167. Ayats, J.R.G.; Calvet, J.V.; Canela, J.M.; Diego-Ayala, U.; Artes, F.F. Power transmitted through a particular branch in mechanisms comprising planetary gear trains and other fixed or variable transmissions. *Mech. Mach. Theory* **2011**, 46, pp. 1744-1754 doi:10.1016/j.mechmachtheory.2011.06.005.
168. Ayats, J.R.G.; Diego-Ayala, U.; Artes, F.F. The singular point transition concept: A novel continuously variable transmission comprising planetary gear trains and a variator. *J. Power Sources* **2012**, 197(1), 125-135 https://doi.org/10.1016/j.jpowsour.2011.07.031.
169. Mantriota, G. Comments on "Power transmitted through a particular branch in mechanisms comprising planetary gear trains and other fixed or variable transmissions". *Mech. Mach. Theory* **2014**, 73, pp. 101-102 http://dx.doi.org/10.1016/j.mechmachtheory.2013.10.011.
170. Xue, H.L.; Liu, G.; Yang, X.H. A review of graph theory application research in gears, *Proc IMechE Part C: J. of Mechanical Engineering Science* **2015**, 30 (10) (2015) 1697– 1714.
171. Esmail, E.L. Meshing Efficiency Analysis of Two Degree-of-Freedom Epicyclic Gear Trains. *J. Mech. Design* **2016**, 138(8) DOI: 10.1115/1.4033693.
172. Wang Y.; Yang, W.; Tang, X.; Lin, X.; He, Z. Power Flow and Efficiency Analysis of High-Speed Heavy Load Herringbone Planetary Transmission Using a Hypergraph-Based Method. *Appl. Sci*. **2020**, 10, 5849; doi:10.3390/app10175849
173. Lévai, Z. Structure and analysis of planetary gear trains. *Journal of Mechanisms* **1968**, 3(3), pp. 131-148 https://doi.org/10.1016/0022-2569(68)90352-2.
174. Freudenstein, F. An Application of Boolean Algebra to the Motion of Epicyclic Drive. *J. Eng. Ind*. **1971**, 93(1): 176-182 https://doi.org/10.1115/1.3427871.
175. Freudenstein, F.; Yang, A.T. Kinematics and Statics of Coupled Epicyclic Spur Gear Trains. *Mech. Mach. Theory* **1972**, 7, pp. 263–375.
176. Willis, R. J.Jr. On the Kinematics of the Closed Epicyclic Differential Gears. *J. Mech. Design* **1982**, 104(4), , pp. 712–719 https://doi.org/10.1115/1.3256415.
177. Gibson, D.; Kramer, S. Symbolic Notation and Kinematic Equations of Motion of the Twenty-Two Basic Spur Planetary Gear Trains. *J. Mech., Trans., and Automation*. **1984**, 106(3): 333-340 (8 pages ) https://doi.org/10.1115/1.3267416.
178. Hsu, C.-H. A graph notation for the kinematic analysis of differential gear trains. Journal of the Franklin Institute **1992,** 329 (5), 859-867 https://doi.org/10.1016/S0016-0032(92)90044-H.
179. Hsu, C.-H.; Lam, K.-T. A New Graph Representation for the Automatic Kinematic Analysis of Planetary Spur-Gear Trains. *J. Mech. Des*. Mar **1992**, 114(1): pp. 196-200 https://doi.org/10.1115/12916916.
180. Ma, R.; Gupta, K.C. Signal Flow Graphs for Spatial Gear Trains. *J. Mech. Des.* **1994** 0161-8458, 116, pp. 326–331.
181. Hsieh, H.-I.; Tsai, L.-W. Kinematic Analysis of Epicyclic-Type Transmission Mechanisms Using the Concept of Fundamental Geared Entities. *J. Mech. Des*. **1996**, 118(2): 294-299 (6 pages) https://doi.org/10.1115/1.2826883.

182. Lang, S.Y.T. Graph-theoretic modelling of epicyclic gear systems. *Mech. Mach. Theory* **2005**, 40, 511–529 doi:10.1016/j.mechmachtheory.2004.12.001.
183. Mathis, R.; Remond, Y. Kinematic and dynamic simulation of epicyclic gear trains, *Mech. Mach. Theory* **2009**, 44, 412–424 doi:10.1016/j.mechmachtheory.2008.03.004.
184. Drewniak, J.; Zawiślak, S. Graph methods in kinematical analysis of multi-speed epicyclic gears. *Int. J. Appl. Mech. Eng*. **2010**, 17(3), 791–798.
185. Drewniak, J.; Zawiślak, S. Linear graph and contour graph based models of planetary gears. *J. Theor. Appl. Mech*. **2010**, 48, 415-433.
186. Zawiślak, S. The graph-based methodology as an artificial intelligence aid for mechanical engineering design. Publishing House Bielsko-Biała University, Bielsko- Biała **2010**.
187. Amirinezhad, S.V.; Uyguroğlu, M.K. Kinematic analysis of geared robotic mechanism using Matroid and T–T graph methods. *Mech.Mach. Theory* **2015**, 88, pp. 16–30 http://dx.doi.org/10.1016/j.mechmachtheory.2015.02.002.
188. Uyguroglu, M.; Tokad, Y. Kinematic Analysis of Robotic Bevel-Gear Trains: An Application of Network Model Approach. *Meccanica* **1998**, 33, 177–194.
189. Uyguroglu, M.; Demirel, H. Kinematic analysis of bevel-gear trains using graphs. *Acta Mechanica* **2005**, 177, 19–27 DOI: 10.1007/s00707-005-0212-8.
190. Drewniak, J.; Kopeć, J.; Zawislak, S. Kinematical and Efficiency Analysis of Planetary Gear Trains by Means of Various Graph-Based Approaches. Editors: Goldfarb, V., Barmina, N. Theory and Practice of Gearing and Transmissions **2016**, pp 263–284,., Part of the book series: Mechan. Machine Science, volume 34 Springer Cham https://doi.org/10.1007/978-3-319-19740-1.
191. Esmail, E.L. A universal kinematic analysis of geared mechanisms. *J. Braz. Soc. Mech. Sci. Eng*. **2017**, 39,2253–2258 DOI 10.1007/s40430-017-0711-2.
192. Yang, A. T.; Freudenstein, F. Mechanics of Epicyclic Bevel-Gear Trains. *J. Eng. Ind.* ***1973,*** 95, 497–502.
193. Wojnarowski, J.; Kopeć, J.; Zawiślak, S. Gears and Graphs. *J. Theoret. Applied Mech*. **2006**, 44, 1, pp. 139-162
194. Liu, C.-P.; Chen, D.-Z.; Tsung Chang, Y.-T. Kinematic analysis of geared mechanisms using the concept of kinematic fractionation. *Mech. Mach. Theory* **2004**, 39, 1207–1221 doi:10.1016/j.mechmachtheory.2004.05.010.
195. Liu, C.-P.; Chen, D.-Z. On the Embedded Kinematic Fractionation of Epicyclic Gear Trains. *J. Mech. Des*. **2000**, 122(4): 479-483 (5 pages) https://doi.org/10.1115/1.1313826.
196. Gao, M.-F.; Hu, J.-B. Kinematic Analysis of Planetary Gear Trains Based on Topology. *J. Mech. Des*. **2018**, 140(1): 012302 (12 pages) https://doi.org/10.1115/1.4038072.
197. Penaud, J.; Alazard, D.; Amiez, A. Kinematic Analysis of Spatial Geared Mechanisms. *J. Mech. Des*. **2012**, 134(2): 021009 (6 pages) https://doi.org/10.1115/1.4005596.
198. Marghitu, D., B. Kinematic Chains and Machine Components Design. Elsevier Academic Press London 2005.
199. Ayats, J.R.G.; Diego-Ayala, U.; Canela, J.M.; Fenollosa, F.; Vivancos, J. Hypergraphs for the analysis of complex mechanisms comprising planetary gear trains and other variable or fixed transmissions. *Mech. Mach. Theory* **2012**, 51, 217–229 doi:10.1016/j.mechmachtheory.2011.07.011.
200. Drewniak, J.; Kopeć, J.; Zawiślak, S. Graph Models of Automobile Gears – Kinematics. *Int. J. Appl. Mech.Eng*. **2010**, 19, 563-573 https://doi.org/10.2478/ijame-2014-0038.
201. Esmail, E.L. Kinematic nomographs of epicyclic-type transmission mechanisms. *Emirates Journal for Engineering Research*, **2007**, 12 (3), 47-55.
202. Esmai, E.L. Nomographs for synthesis of epicyclic-type automatic transmissions. *Meccanica* **2013**, 48, 2037–2049 DOI 10.1007/s11012-013-9721-z.
203. Esmai, E.L. Nomographs and Feasibility Graphs for Enumeration of Ravigneaux-Type Automatic Transmissions. *Adv. Mech. Eng*. **2013**, Article ID 120324, 15 pages http://dx.doi.org/10.1155/2013/120324.
204. Hussen, H.A.; Esmail, E.L. Application of incidence matrix to topological structure and kinematic analysis of multi-planet gear trains. *Results in Engineering* **2021**, 12, 100305 https://doi.org/10.1016/j.rineng.2021.100305.
205. Esmail, E.L. Teaching Planetary Gear Trains with the Aid of Nomographs. *Adv. Mech. Eng*. **2013**, Article ID 978418, https://doi.org/10.1155/2013/978418
206. Talpasanu,I.; Yih, T.C.; Simionescu, P.A. Application of Matroid Method in Kinematic Analysis of Parallel Axes Epicyclic Gear Trains. *J. Mech. Des*. **2006**, 128(6),1307-1314 (8 pages) https://doi.org/10.1115/1.2337310.

207. Mruthyunjaya, T.S.; Raghan, M.R. Computer-aided analysis of the structure of kinematic chains. *Mech. Mach. Theory*. **1984**, 19,3, pp. 357-368 https://doi.org/10.1016/0094-114X(84)90070-3.
208. Ke, T.; Ding, H.; Gong, C.; Geng, M. Configuration synthesis of nine-speed automatic transmissions based on structural decomposition. *Mech. Mach. Theory* **2021**, 164, 104421 https://doi.org/10.1016/j.mechmachtheory.2021.104421.
209. Ding, H.; Cai, C.; Chen, Z.; Ke, T.; Mao, B. Confguration Synthesis and Performance Analysis of 9-Speed Automatic Transmissions. *Chin. J. Mech. Eng*. **2020**, 33:50 https://doi.org/10.1186/s10033-020-00466-y.
210. Buchsbaum, F.; Freudenstein, F. Synthesis of Kinematic Structure of Geared Kinematic Chains and Other Mechanisms. *J. Mech.* **1970**, 5(3), pp. 357–392 https://doi.org/10.1016/0022-2569(70)90068-6.
211. Yin, C.; Tang, D.; Deng, Z. Research on configurations of multi-axis speed-differential mechanisms based on 2K-H gear train. *Mech. Mach. Theo*ry **2020**, 148, 103783 https://doi.org/10.1016/j.mechmachtheory.2020.103783.
212. Wojnarowski, J.; Drewniak, J.; Kądziołka, T.; Kopeć, J.; Stańco, K.; Zawiślak, S. Application of Contour Equations to Kinematic Analysis of Complex and Compound Planetary Gears. T. Uhl (ed.), Advances in Mechanism and Machine Science, Mechanisms and Machine Science 73, Springer Nature Switzerland AG 2019 https://doi.org/10.1007/978-3-030-20131-9_98.
213. Zhou, H.; Wang, L.; Lu, Z.; Qian, J.; Zhang, H.; Zhao, Y.; Cheng, Z.; Wang, X. Transmission Parameter Design and Characteristic Analysis of Three-Row Parallel Planetary Gear HMCVT. *Machines* **2022**, 10, 740. https://doi.org/10.3390/machines10090740.
214. Wu, J.; Yan, H.; Liu, S.; Zhang, Y.; Tan, W. Bond Graph-Based Approach to Modeling Variable-Speed Gearboxes with Multi-Type Clutches. *Appl. Sci*. **2022**, 12, 6181. https://doi.org/10.3390/app12126181.
215. Tsai, M.-C.; Huang, C.-C.; Lin, B.-J. Kinematic analysis of planetary gear systems using block diagrams. *J. Mech. Des*. **2010**, 132(6), p. 065001.
216. Tian, L.; Li-qiao, L. Matrix System for the Analysis of Planetary Transmissions. *J. Mech. Des*. **1997**, 119(3): pp. 333-337 https://doi.org/10.1115/1.2826352.
217. Liu, F.; Wu, W.; Hu, J.; Yuan, S. Design of multi-range hydro-mechanical transmission using modular method. *Mechanical Systems and Signal Processing*. 2019, 126, pp.1-20 https://doi.org/10.1016/j.ymssp.2019.01.061.
218. Raghavan, M. The Analysis of Planetary Gear Trains. *J. Mechanisms Robotics*. **2010** DOI: 10.1115/1.4001092.